iScience

CellPress
OPEN ACCESS

Article

Astrocyte's self-repairing characteristics improve working memory in spiking neuronal networks

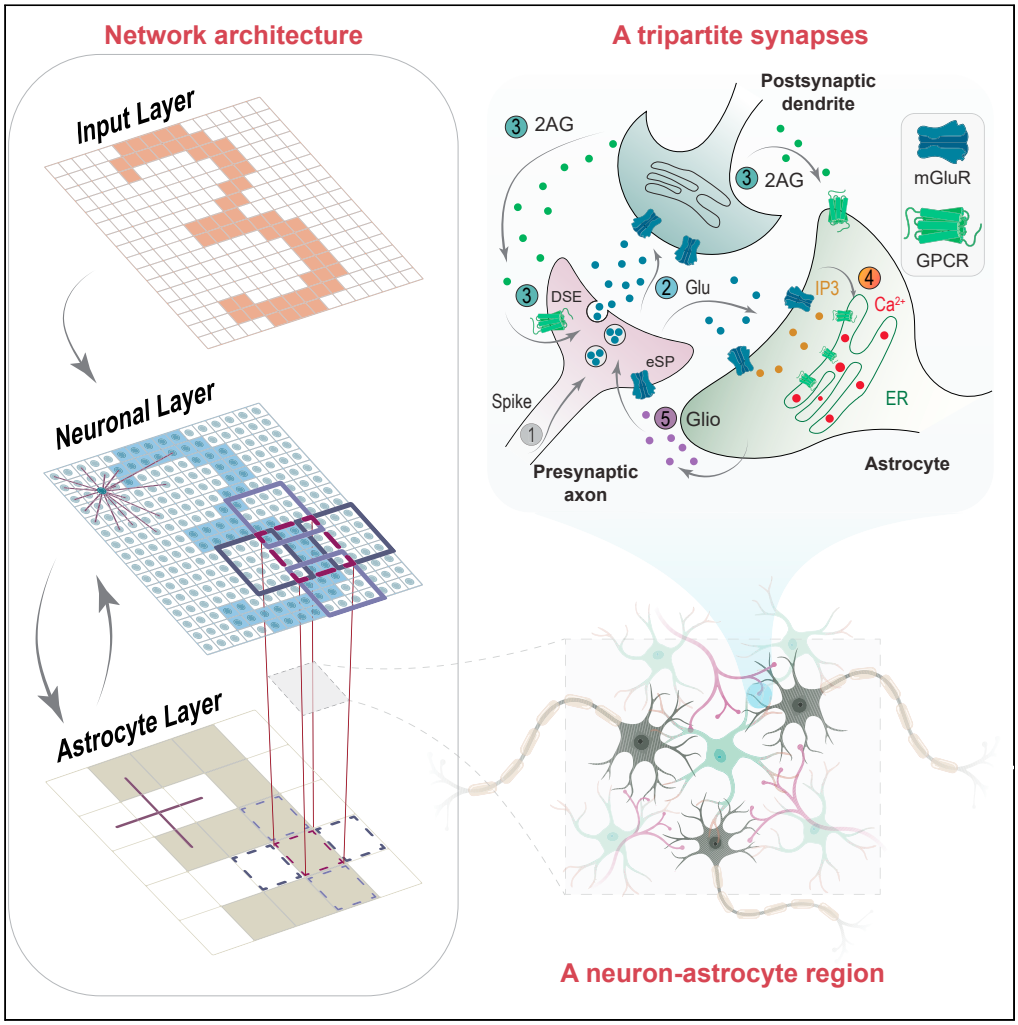

Pedram Naghieh, Abolfazl Delavar, Mahmood Amiri, Herbert Peremans

ma_amiri_bme@yahoo.com (M.A.)
herbert.peremans@uantwerpen.be (H.P.)

Highlights

A self-repairing (SR) algorithm for a neuron-astrocyte network is proposed

In a synaptically impaired network SR process improves working memory (WM) performance

Intercellular astrocytic Ca^{2+} propagation facilitates the SR mechanism and WM function

Naghieh et al., iScience 26, 108241
December 15, 2023
https://doi.org/10.1016/j.isci.2023.108241

iScience

CellPress
OPEN ACCESS

Article

Astrocyte's self-repairing characteristics improve working memory in spiking neuronal networks

Pedram Naghieh,[1] Abolfazl Delavar,[1] Mahmood Amiri,[1,2,3,*] and Herbert Peremans[2,*]

SUMMARY

Astrocytes play a significant role in the working memory (WM) mechanism, yet their contribution to spiking neuron-astrocyte networks (SNAN) is underexplored. This study proposes a non-probabilistic SNAN incorporating a self-repairing (SR) mechanism through endocannabinoid pathways to facilitate WM function. Four experiments were conducted with different damaging patterns, replicating close-to-realistic synaptic impairments. Simulation results suggest that the SR process enhances WM performance by improving the consistency of neuronal firing. Moreover, the intercellular astrocytic $[Ca]^{2+}$ transmission via gap junctions improves WM and SR processes. With increasing damage, WM and SR activities initially fail for non-matched samples and then for smaller and minimally overlapping matched samples. Simulation results also indicate that the inclusion of the SR mechanism in both random and continuous forms of damage improves the resilience of the WM by approximately 20%. This study highlights the importance of astrocytes in synaptically impaired networks.

INTRODUCTION

Glial cells serve as the primary facilitators of communication between neurons, contributing to the orchestration of the brain's intricate processes.[1] Astrocytes, one of the glial cells in the central nervous system (CNS), have many roles which emerge from the developmental phase of the brain.[2] They participate in key aspects of brain functions such as neuronal metabolism, synaptogenesis,[3] homeostasis of the extracellular milieu, and cerebral microcirculation.[4] Astrocytes can exhibit both local and whole-cell responses which differ in amplitude, duration, signaling pathways, functions, and location.[5–7] These cells encode information through localized "spotty" calcium microdomains within specific processes and endfeet, which contribute to a significant portion of internal calcium elevations.[8,9] Global calcium signaling in astrocytes incorporates the entire astrocyte cytoplasm and involves various mechanisms, including extracellular calcium, ionotropic receptors, metabotropic receptors, and other channels such as transient receptor potential A1 (TRPA1) channels.[9–11] Localized calcium transients in perisynaptic processes and endfeet regulate synaptic function and blood flow, modulating communication with neurons in a targeted manner.[12] Whole-cell calcium oscillations trigger gliotransmitter release, leading to synchronized activities across astrocyte network and modulating synapses on a broader scale.[7,13] These signaling pathways facilitate localized events within microdomains, potentially encoding distinct astrocyte functions that span from synaptic modulation to the regulation of brain circuits and behavior.[8] Additionally, they contribute to higher cognitive functions such as working memory (WM) by maintaining "online" information during delay periods in both healthy and diseased brain conditions.[14] Although there are multiple computational models of spiking neuron-astrocyte networks (SNAN) that explain the WM mechanism in a healthy condition,[15–19] none of them describe how these cells can facilitate the WM function in a synaptically impaired network.

Nearly three decades ago, astrocytes were recognized as regulators of synaptic function in what is referred to as "tripartite synapses".[20–22] In these domains, astrocytes mediate the interaction between presynaptic neurons (PrSNs) and postsynaptic neurons (PoSNs) through the uptake of neurotransmitters and release of gliotransmitters, also known as perisynaptic processes.[23] In the tripartite synapse, PrSNs release neurotransmitters such as glutamate from axonal terminals, targeting PoSNs and astrocytes.[13,24,25] When the PoSN fires, it releases endocannabinoids such as 2AG (2-arachidonyl glycerol) from its dendritic terminals, targeting cannabinoid receptors CB1 and CB2, which are a type of G protein-coupled receptors (GPCRs), on PrSNs and adjacent astrocytes.[26,27] This signal has different effects depending on the targeted cells; it serves as an inhibitory signal for PrSNs, while having a positive effect on neighboring astrocytes, inducing them to release gliotransmitters.[26,27] In the healthy state, the balance of inhibitory and excitatory substances within the axonal terminals of PrSNs is nearly neutral.[28,29] However, if synapses become damaged, this balance is disturbed, leading to the modulation of the transmission probability (PR) in both healthy and damaged synapses.[28,29] If the incoming signal from astrocytes overcomes this imbalance, it results in the positive modulation of synapses, which can be interpreted as the self-repairing (SR) process of the damaged or low PR synapses.[26]

[1]Medical Technology Research Center, Institute of Health Technology, Kermanshah University of Medical Sciences, Kermanshah, Iran
[2]Department of Engineering Management, University of Antwerp, Antwerp, Belgium
[3]Lead contact
*Correspondence: ma_amiri_bme@yahoo.com (M.A.), herbert.peremans@uantwerpen.be (H.P.)
https://doi.org/10.1016/j.isci.2023.108241

One of the first computational models for the SR concept was proposed by J. Wade[30] and later improved by incorporating a learning rule.[31] However, this model functions optimally only with a probabilistic neuron model and a random input. Since the PR-based SR algorithm is embedded within a probabilistic neuron model, it is difficult to use it with other neuronal models. In this article, the SR algorithm is improved to be compatible with the non-probabilistic neuronal models at the network level, receiving deterministic inputs in selective intervals. The proposed algorithm, referred to as Balance of Firing (BoF), is inspired by the core mechanism of SR, which involves balancing excitatory and inhibitory substances in the synaptic buttons. One of the key novelties in the presented BoF-based SR algorithm is the consideration of dynamic local astrocyte activity. These local activities depend on the synaptic activities of neurons referred to as Strength of Input (SoI). Therefore, by correlating the electrochemical signaling between neurons with the localized biochemical modulation of astrocytes, the proposed SR algorithm can be applied to the SNAN models operating with deterministic inputs.

Astrocytes release various synaptogenic factors, including thrombospondins, neuroligins, glypicans, and TNF-alpha, to control synaptogenesis.[3,32] The release of these factors can be influenced by external stimulation and neuronal cues, which in this case is the release of 2AG and glutamate due to neuronal activities, highlighting the complex interplay between astrocytes and neurons in the formation and maturation of synapses.[3,32] The release of 2AG from neurons also plays a role in the regulation of synaptogenesis by affecting the release or function of these astrocyte-derived factors. For instance, the activation of astrocytic TRPA1 channels by 2AG is involved in modulating these signaling pathways.[10,33]

Short-term memory involves retaining a small amount of information in mind. When this information is utilized in the execution of cognitive tasks, it is referred to as working memory (WM).[34] Information from visual,[35,36] temporal,[37] and sensory afferents[38–40] emerges in the form of coordinated activity of the neurons in the CNS.[41] This information is temporarily stored through the modulation of synaptic strength and the regulation of intracellular calcium concentration in astrocytes.[42] Specifically, this process involves microdomain events, perisynaptic processes, and endfeet regulations mediated by ionotropic receptors, metabotropic receptors, and other channels such as TRPA1.[8,10] The activation of astrocytic TRPA1 channels by 2AG is involved in the regulation of astrocyte basal calcium levels and long-term potentiation via constitutive d-serine release.[10,33] These signaling mechanisms mediate microdomain events that may encode specific astrocyte functions, such as their local and global activities for WM and SR processes. Therefore, it is valuable to incorporate both glutamate and 2AG signals from neurons in the conventional SNAN models, particularly for the WM mechanism.

Encoded information inside astrocytes can last from a dozen seconds[43,44] to a dozen minutes,[45–47] contributing to both long- and short-term synaptic plasticity. This limited temporary memorized information can be recalled if the appropriate cue sample is applied to the network. In the early stages, several computational models containing exclusively neuronal networks in various forms and topologies, utilizing a learning rule for synaptic plasticity were presented to model the concept of WM.[48–53] Subsequent WM models have attempted to include the role of astrocytes.[15–18] In these SNAN models, the WM function is conceptualized through whole-cell astrocytic modulation triggered by strong synchronous neuronal activity.

This work integrates both SR and WM concepts mediated by astrocytes in a large-scale SNAN model for the first time. To achieve this, astrocytes detect two types of activities and respond differently to them. The local activity of astrocytes is adapted by the proposed BoF-based SR algorithm, while their whole-cell activity is considered by modifying the WM algorithm from one of the previous models.[15] Additionally, two depletion factors are added to the astrocyte model for their local and whole-cell activities. These factors act as an extra decay rate for Ca^{2+} when local or whole-cell astrocyte activities initiate. This is also in accordance with some of the design methodologies of previous works such as the Tsodyks-Markram model[54] for synapse dynamics and the De Pitta models[18,55] for astrocyte dynamics. Furthermore, a mechanism for the glutamate release from the neurons is designed, which is ideal for modeling how synaptic damage affects the neurotransmitter release. To test the model, four experiments with various forms of synaptic damage are designed to evaluate the performance of astrocytic SR mechanism on the WM function. In the first experiment, the network is tested in the healthy status, demonstrating that the proposed changes to the neuron and astrocyte dynamics do not interfere with the WM performance. The second experiment indicates that the proposed BoF-based SR algorithm operates properly by increasing the SR activities only in the damaged areas when stimulated by the input samples. Experimental data suggest that the shape of the synaptic diseases is in the form of spongiform changes in the nervous system[56]; therefore, the last two experiments try to impair the network similarly to the observed experimental findings in the continuous and random damage modes. Simulation results suggest that the addition of the SR mechanism in all conditions facilitates the retrieval of items for the WM function. In the continuous damage mode, the inclusion of SR process increases the resilience of the network from 38% to 62% damage. Similarly, in the random damage mode, there is a 20% improvement in the resilience of the WM, keeping this mechanism functional up to 60% random synaptic damage.

RESULTS

Network structure

The architecture of the model incorporates three layers of two-dimensional networks representing input layer, neuronal, and astrocyte networks[15] (Figure 1A). Each pixel of the 79 x 79 input layer connects to a neuron in the 79 x 79 neuronal layer. The interconnections within the Izhikevich neuronal layer involve excitatory neurons that form sparse connections, with each neuron having a limited range for establishing these connections. It is assumed that each PrSN only forms one connection to another PoSN. Each neuron is randomly connected to 40 other neurons. Neurons in this model can only communicate with glutamate and 2AG to other neurons and neighboring astrocyte(s). While astrocytes are in contact with 270,000–2 million synapses in the human brain,[57,58] an individual cortical astrocyte contacts an average of 4–8 neuronal soma in the cortex.[59] This allows the astrocyte to integrate and coordinate a unique volume of synaptic activities. Based on these

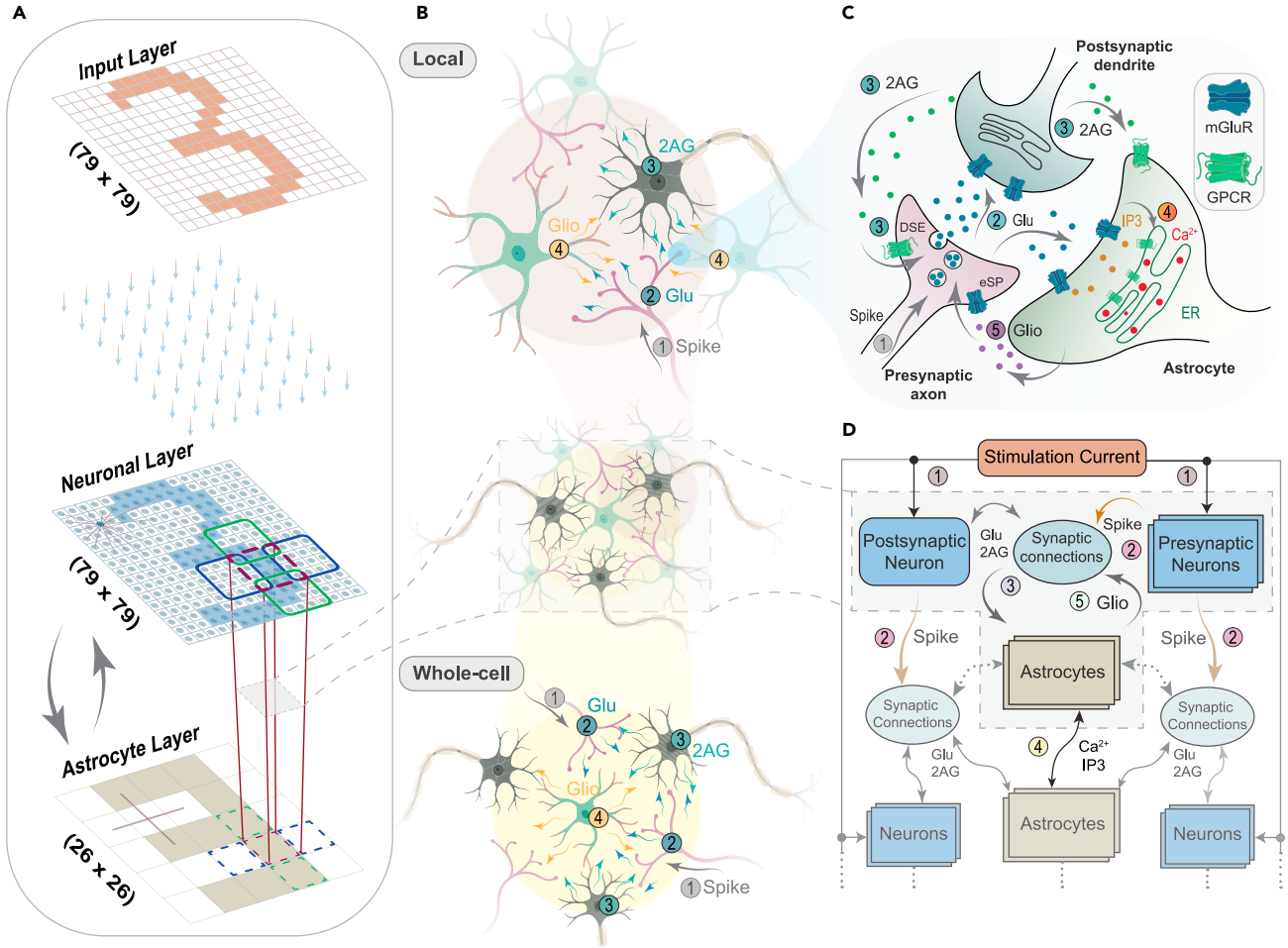

Figure 1. Model functionality from various perspectives (A) 2D lattice networks, (B) neuron-astrocyte region, (C) tripartite synapses, and (D) postsynaptic neuron.

(A) The model comprises of three two-dimensional networks corresponding to input layer, neuronal and astrocyte networks. The input layer is parallelly connected to the neuronal layer. Interconnections of the Izhikevich neuronal layer consist of synaptically coupled excitatory neurons with a limited range for each neuron to form sparse connections. Astrocytes are interconnected with up to four other astrocytes through gap junctions. Each astrocyte interacts with a 4 x 4 rectangular region of neurons, sharing four overlapping, 1 x 4 tiles, with adjacent astrocytes.

(B) In a neuron-astrocyte region, the concepts of local activity of astrocytes (top) and their whole-cell activity (bottom) are illustrated.

(C) The sequence of released substances and interactions in the tripartite synapse is indicated.

(D) A simplified representation of the model from a PoSN perspective. (1) Input is simultaneously applied to all neurons, (2) causing spike activities and (3) initiating the release of glutamate and 2AG in synaptic clefts. Following the production of IP_3 and Ca^{2+}, (4) they can diffuse via gap junctions to the adjacent astrocytes. (5) As Ca^{2+} oscillations inside the astrocytes reaches specific levels, they can release gliotransmitters to the synapse.

experimental findings, the astrocyte network in this model is organized into a two-dimensional lattice (26 x 26) with nearest-neighbor connectivity. Each astrocyte interacts with a 4 x 4 rectangular region of neurons with the overlapping of 1 x 4 tile of neurons with its adjacent astrocytes (Figure 1A). Therefore, in a neuron-astrocyte zone, corner neurons communicate by four astrocytes, edge neurons interact with two astrocytes, and middle neurons communicate by one astrocyte.

When a PrSN is stimulated first (Figure 1C), it releases glutamate from its axonal terminal targeting postsynaptic and astrocytic metabotropic glutamate receptors (mGluRs) to convey its message. If this excitation is strong enough, the PoSN fires and releases a puff of 2AG from its dendritic terminal targeting type 1 Cannabinoid Receptors (CB1Rs) on both PrSNs and astrocytes.[26,60] The main purpose of this signal is to depolarize its PrSNs directly and reduce their transmission probability (probability of glutamate release) as a sign of successful action potential due to their previous glutamate release events.[26,28] This signal is termed "Depolarization-induced Suppression of Excitation (DSE)"[27] (Figure 1C). As the released glutamate and 2AG from pre- and post-synaptic neurons bind with the receptors on astrocytes, they trigger the production of inositol 1,4,5-trisphosphate (IP_3) inside astrocytes, eventually leading to the elevation of internal calcium ions. Generated Ca^{2+} and IP_3 can be diffused to other astrocytes via Cx43 gap junctions.[61–63] Therefore, information coming from the input layer which is converted to spikes in the neuronal network is encoded and propagated within the astrocytic network in the form of Ca^{2+} waves.

When intracellular Ca^{2+} concentration reaches a certain level, astrocytes can release gliotransmitters such as glutamate, targeting mGluRs on neurons. The released 2AG from PoSNs can directly impose an inhibitory impact on the PrSNs, but it can also provoke an indirect excitatory impact on PrSNs through the locally released gliotransmitter by astrocytes. This indirect excitatory signaling is known as "endocannabinoids mediated Synaptic Potentiation (e-SP)"[26] (Figure 1C). Although both glutamate and 2AG from neurons contribute to promoting calcium ions in astrocytes, leading to the release of gliotransmitter and generation of the eSP signal, it is only 2AG that can lead to both potentiation and inhibition of PrSNs. In this model, astrocytes can release local gliotransmitter (Gli_{Local}) as they detect any synaptic activity if they have Ca^{2+} levels greater than 0.1 μM (Figure 1B). Synaptic activity is modeled by calculating SoI for each neuron (Equation 7). This local activity of astrocytes serves as the eSP signal for the SR mechanism. In an impaired network, the local activity of neurons (SoI) and consequently the local activity of astrocytes (Gli_{Local}) are reduced based on the damage intensity. However, SR activities increase as the damage increases because the DSE signal depends only on the released 2AG from PoSN, while the eSP signal depends on the astrocytic Ca^{2+} supplied by multiple neurons and neighboring astrocytes. On the other hand, whole-cell gliotransmitter release (Gli_{Global}) from astrocytes is triggered when they detect strong synchronous activity while having Ca^{2+} levels greater than 0.15 μM.[64,65] Synchronous activity is defined as having more than half of the connected neurons to an astrocyte simultaneously spiking.[64–66] This whole-cell activity impacts all the connected neurons to that astrocyte (Figure 1B).

To investigate the effect of the SR mechanism in the presented SNAN with WM, four experiments are designed. Throughout all experiments, the delayed matching to sample (DMS)[67] aspect of the WM model is preserved. The only difference is in the type of damage and the presence of SR modulation. Damage is imposed on the neuronal network to simulate a simplified stationary state of a neurodegenerative disease, meaning that the damage does not develop during any of the simulations. To model the effects of damage, a new mechanism for glutamate release is presented which functions based on the synaptic activity. To represent the impact of local and whole-cell activities on the calcium concentration of astrocytes, two depletion factors were added to the previously known Ullah model (Equation 15).

To model damage, two ST (strength) factors are utilized to modulate the efficacy of neuronal interactions. In healthy conditions, the default value for these parameters is set to one; any imposed damage reduces this value to a quantity between zero and one. Parameter ST1 modulates synaptic connections, while ST2 affects glutamate release and noise current. The 2AG is indirectly influenced by the reduction in the frequency of neuronal firing. These ST factors are set based on the damage mode. In the random damage mode, ST1 is selected randomly for each synapse. In the pattern-specific damage mode, ST1 for all connections of neurons is defined based on the intensity and formation of a damaging pattern. In both damage modes, the variable ST2 for each neuron is calculated by averaging ST1.

The proposed self-repairing algorithm

The concept of the SR mechanism begins with the modulation of PrSNs and astrocytes by the released 2AG from PoSNs in the close proximity. To model this process at the network level, four signals are necessary. The first signal is a direct inhibitory modulation from the PoSN to PrSN boutons (DSE). The second signal is the indirect excitatory modulation to the PrSN by astrocytes (eSP) which results from local astrocytic activity (Gli_{Local}). Both DSE and eSP signals are consistent across PR-based and BoF-based SR algorithms. The third signal encodes the level of synaptic activity to adapt the local activity of astrocytes based on the neuronal activities, which is crucial for extending the SR algorithm to the network level, operational in selective intervals. The fourth signal represents the health status of the synapses, denoted as $PR_0^{(k)}$ in the PR-based and ST_k in the BoF-based SR algorithms. The last two signals must be designed to the specific architecture of the neuronal network. In addition to these four signals, the SR algorithm requires two threshold values. The first one is the minimum required Ca^{2+} concentration for the initiation of the local activity of astrocytes ($[Ca^{2+}]_{Thr(SR)}$). The second value is the threshold of SR activities, defined by introducing a noise margin for the acceptable imbalance between DSE and eSP values (BoF_{th}). For better understanding of the SR algorithm, it is best to describe a system with SR mechanism as being in one of these three states. The first state represents a healthy condition, the second state signifies the onset of damage detection (referred to as the first SR step), and the third state encompasses the SR process itself (referred to as the second SR step). Indeed, the damage detection and the execution of the SR process result from internal feedback loops.

In Wade's model,[30] the SR mechanism was demonstrated in a model with four neurons and one astrocyte. Damage was imposed on the system by selectively reducing the default transition probability value ($PR_0^{(k)}$) of some synaptic connections from the PrSNs. Upon inducing damage, the first step of the SR algorithm is triggered, resulting in decreased 2AG release and consequently reduced DSE production. In that model, any reduction in the 2AG release has no impact on the local activity of astrocytes and produced eSP. Therefore, in the PR-based SR algorithm utilized in previous works, everything is attached to the eSP signal which always remains constant. Under this assumption, SR activities occur through an increase in the PR value due to a decrease in the incoming inhibitory signal from the PoSN. An increase in the PR value of both healthy and unhealthy synapses triggers the second step of the SR algorithm, leading to an increase in the probability of postsynaptic firing. While interventions in unhealthy synaptic connections have little or no significant effect, increased activity in healthy connections compensates for the shortcomings of unhealthy ones.

The major problem with a constant eSP signal arises when extending the model to the network level, particularly when dealing with multiple PrSNs and astrocytes that operate within specific time intervals. As the network size increases, certain PrSNs may not fire (i.e., do not receive input), resulting in some inactive synapses (i.e., not releasing any glutamate). Consequently, the eSP signal should not indiscriminately regulate synaptic activities, as it would be unable to differentiate between "inactive" and "impaired" connections. This demands for introducing a new signal that adjusts the local activity of astrocytes based on the synaptic activities. In the proposed model, *SoI* carry out this role, as it computes the relative number of activated synapses at a given time (Equation 7). It is important to note that SoI is not a constant factor for all neurons; it is calculated individually for each neuron and normalized based on the number of existing connections. In the proposed model,

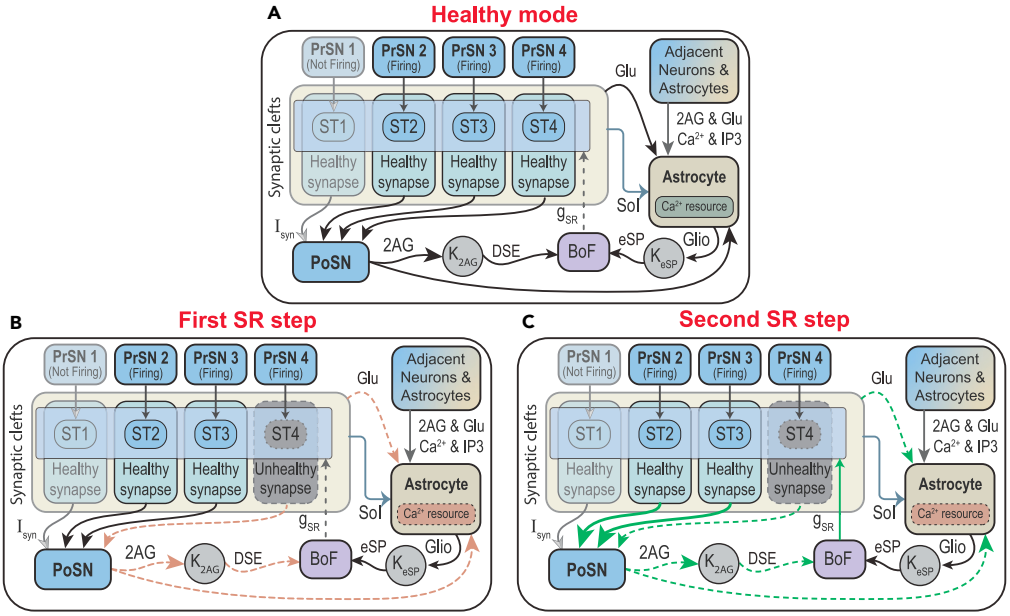

Figure 2. BoF-based SR algorithm

(A) In the neural network, some neurons can receive input and fire, while others may be in the resting states. Therefore, local astrocytic activities are adjusted based on synaptic activities (SoI). Under healthy conditions, astrocytes' Ca^{2+} increases, and the SR signal (g_{SR}) is occasionally applied to the system by evaluating the balance between DSE and eSP signals.

(B) Inducing any damage to the system reduces the release of 2AG and glutamate, leading to a decrease in DSE and Ca^{2+} production as shown by dashed brown arrows.

(C) Induced minor damages slightly affect the SoI signal, resulting in a nearly constant local astrocytic activity. This leads to have higher eSP than DSE values, which triggers the SR process by applying the g_{SR} signal to all synaptic connections as shown by green arrows.

the number of presynaptic connections varies for each neuron, leading to unique SoI values for each neuron. Experimental results suggest that neuron-astrocyte interactions are non-linear.[68] Hence, $SoI_{Syn(N)}$, a non-linear form of *SoI*, is defined and utilized for adjusting local astrocytic activity (Equation 8). Minor damage to synapses has a limited impact on the $SoI_{Syn(N)}$ signal, as it operates almost independently from the health status of synapses. However, significant damages (i.e., ST = 0 or close to 0) trigger a chain of reactions in the neuronal network activities, inevitably reducing synaptic and local astrocyte activities.

In the BoF-based SR algorithm (Figure 2A), inducing any damage to the axonal terminals of PrSNs with ST factors causes a reduction in the frequency of 2AG and glutamate release. This has a minor impact on the local activity of astrocytes, resulting in a slight effect on the eSP signal but significantly reducing the produced DSE signal. This irregularity is detected in the first SR step (Figure 2B). In the second step of the SR algorithm, since astrocytes function based on activated synapses, the released eSP signal remains mostly intact, while DSE is constantly decreasing, resulting in an imbalance in the BoF value. When BoF passes a certain threshold, the SR activities (g_{SR}) is initiated, leading to an increase in the synaptic current of the activated synapses due to a lower DSE value in the presynaptic axonal terminals (Figure 2C). It is important to note that, in the PR-based SR algorithm, excitation and inhibition were modeled by increasing and decreasing the PR value, respectively. In the BoF-based SR algorithm, excitation is modeled by receiving the g_{SR} signal, and inhibition is modeled by taking the g_{SR} signal away.

Experiment 1 - Healthy network with self-repairing signal

WM is characterized by the emergence of persistent activity in the absence of input stimulation. When this persistent activity arises after a brief delay, the WM model is referred to as the DMS-WM type.[69] Current hypotheses for the delay in DMS-WM phenomena are associated with the slow rise time of calcium in astrocytes and their slow activities.[70] In the first experiment, the model is presented in healthy conditions to understand the underlying mechanisms of DMS-WM with SR process. There are four input samples with a distortion level of 5% during the training phase and eight additional samples (four matched and four non-matched) with a distortion level of 20% in the testing phase (Figure 3A). To address the matched samples (already seen), they are referred to as M0, M1, M2, and M3 to represent their respective numerical values while non-matched samples (new) are referred to as NM. During the training phase, items are applied for a duration of 0.2 s with a 0.1s interval between each sample. Items in the testing phase are applied for 0.15 s. If these samples are recognized based on WM the neurons continue to fire for an additional 0.1 s influenced solely by the modulation of the astrocytes. A 0.25 s gap separates items in the testing phase. The samples exhibit approximately a 35% overlapping ratio. The parts with a higher overlapping ratio can be discerned from the Ca^{2+} snapshot before test since they have higher concentration of Ca^{2+} (Figure 3D). The connectivity within the neuronal network follows the distance

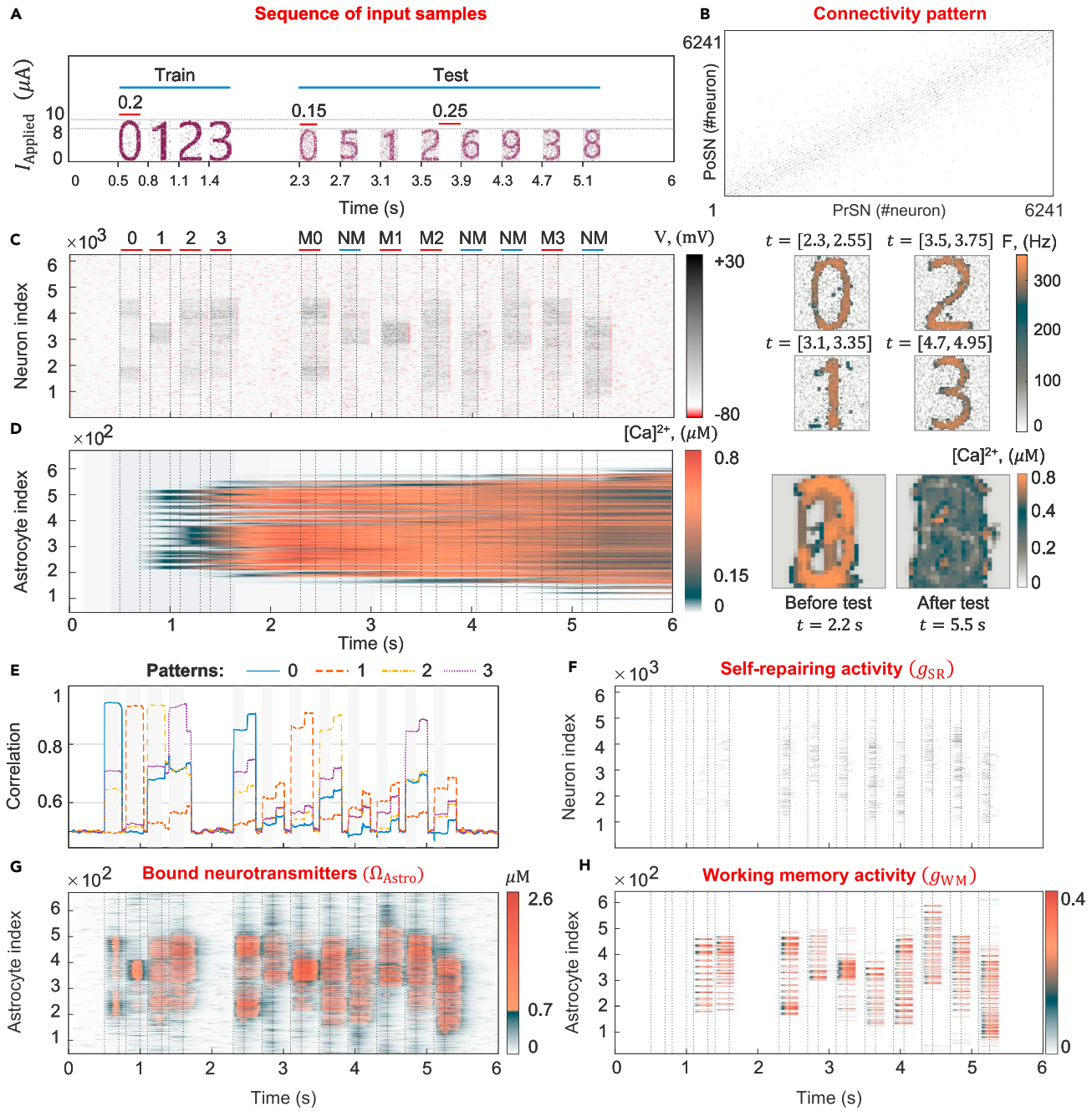

Figure 3. Experiment 1 – Performance of the healthy network

(A) Four samples of "0" to "3" with 5% distortion are selected for the training phase (indicated as M0 – M3). In the test phase, those four samples in addition to four non-match samples (indicated as NM) with 20% distortion are applied to the network.

(B) Connectivity pattern of PrSNs with PoSNs follows the distance dependency rule.

(C) Neuronal membrane potentials are illustrated in two color codes to identify when neurons are in the hyperpolarization period. Frequency snapshots for the matched samples in the 250 ms of the WM interval in the test phase are identified.

(D) In the astrocyte network, the 0.15 μM calcium threshold is used for the whole-cell activity, which leads to the WM. Snapshots of the calcium concentration before and after the training phase indicate the propagation of Ca^{2+} in the astrocytic network.

(E) Calculated correlation is the highest for the matched samples in the test phase.

(F) SR activities emerge as the calcium concentration passes the 0.1 μM threshold.

(G) A monotonic input for astrocytes is considered as long as the total bound glutamate and 2AG are above the 0.7 μM threshold.

(H) When astrocytic Ca^{2+} passes the 0.15 μM threshold, they can apply their whole-cell activity if they detect strong synchronous neuronal activities.

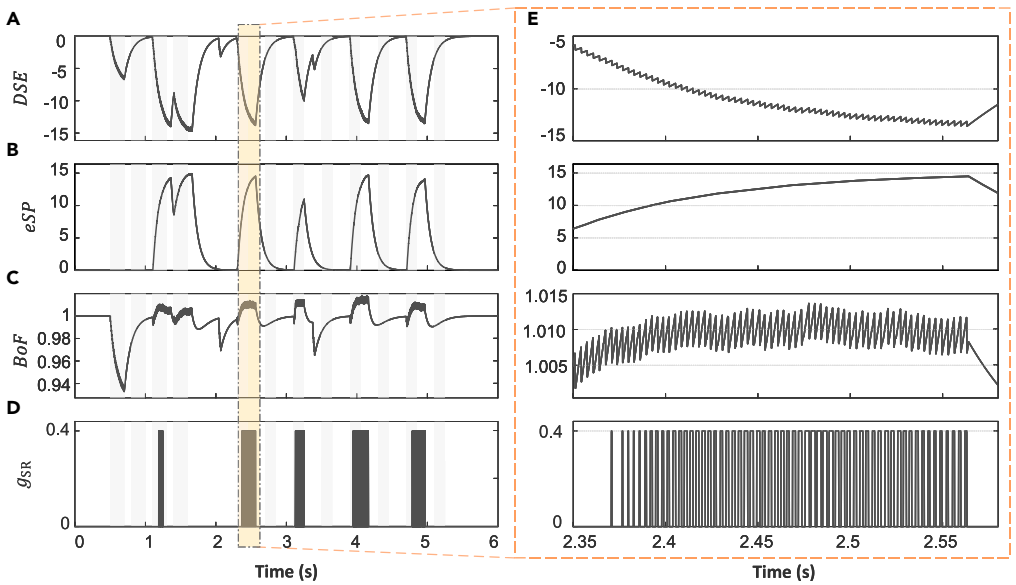

Figure 4. Single-cell behavior of a neuron with synaptic impairment

(A) DSE signal is calculated by multiplying the 2AG signal by a negative factor.

(B) eSP signal is calculated by multiplying the locally released gliotransmitter by a positive factor.

(C) Balance of Firing (BoF) is evaluated by comparing the DSE with the eSP signal. Since the local activity of astrocytes requires 0.1 μM of Ca^{2+} to initiate, eSP has no value from 0.5 to 1 s, leading to low values of BoF.

(D) SR signal (g_{SR}) is applied to the neurons if the BoF signal passes the 1.01 threshold.

(E) All signals are magnified.

dependency rule, which states that each neuron is more likely to form connections with closer neurons rather than those are farther away (Figure 3B). The encoded information in the neurons takes the form of a burst with a firing frequency between 280 and 290 Hz (Figure 3C). This frequency is calculated within the 250 ms window of the WM interval during the testing phase for each sample.

Intracellular astrocytic Ca^{2+} levels can increase due to various sources; in this model, the primary cause is the release of glutamate and 2AG in the tripartite synapses. Astrocytic whole-cell WM activities emerge when astrocytes detect strong synchronous neuronal activity and have enough internal Ca^{2+} concentration.[41,64,66] To model this interaction, if the total bound glutamate and 2AG from at least half of the connected neurons to an astrocyte go beyond the 0.7 μM threshold (Equation 11), a monotonic input (A_Ω) is considered for the astrocytes (Equations 12 and 13; Figure 3G).[71] In this manner, the delay of the DMS-WM is modeled through two components: first, the rise time of the accumulated released neurotransmitter in the tripartite synapse to 0.7 μM, and second, the calcium rise time to a specific level (0.1 μM for SR and 0.15 μM for WM). By comparing the Ca^{2+} levels within the astrocyte network before and after the test phase, it can be deduced that the astrocyte network has the highest Ca^{2+} concentration at 2.2 s before the test phase. After the test phase, at 5.5 s, Ca^{2+} has propagated through the astrocyte network via gap junctions or decayed with its natural rate indicating that the network is forgetting the cued samples as the time passes.

Since the current version of the WM model[15] does not consider different intensity levels of neural activity evoked by the gliotransmitter release in time and space[72]; both WM and SR activities (g_{WM} and g_{SR}) are modeled using rectangular-shaped signals with specific amplitudes (Equations 23 and 25). As these signals are shaped such as rectangular pulses, their integrals can be calculated for quantification purposes. Note that whole-cell astrocytic activity is triggered by intense neuronal activity and impacts all connected neurons, while local astrocytic activity occurs around single neuron only (Figure 1B). Astrocytes' local activity is realized as the eSP signal in presynaptic boutons. Indeed, if the balance between eSP and DSE signals is disturbed (a tolerance of 0.01 for BoF is considered (Figure 4)), they receive an extra g_{SR} signal as SR process. Additionally, intermittent SR signal shown in Figure 3F can also be interpreted as a neurotransmitter recycling mechanism by astrocytes since this process also stems from the local activities of astrocytes. The g_{SR} oscillations is attributed to the simultaneous rise of both eSP and DSE signals. This creates a competition between these two signals in presynaptic boutons, resulting in a whipsawed action of the BoF signal when astrocytes produce local activities (Figure 4E).

To evaluate the accuracy of the detected WM in the test phase, the correlation is computed for each sample. This variable is calculated by comparing the emerging neuronal activity with the activity caused by the input samples[15] (Equation 26). Since items in the test phase have a 20% distortion, a 0.8 level is selected as the acceptable correlation threshold. For matched samples in the test phase, computed correlations are all above the threshold (Figure 3E). Moreover, robustness is defined by calculating the integral under the WM interval of the computed correlation. In this case, the extra 0.1 s of neural network firing due to astrocytic modulation is considered for this task. Calculated robustness for samples 0 to 3 are 0.91, 0.93, 0.9, and 0.88, respectively. It is also worth noting that the sudden increase in correlation is due to the absence

of input during that interval, as there is a 20% distortion in the stimulation current. In conclusion, the simulation results from the healthy network depicted in Figure 3 confirm that incorporating the proposed SR process, the glutamate release mechanism, and modifications in astrocytic Ca^{2+} depletion due to local and whole-cell activities do not negatively impact the performance of the WM.

Experiment 2 - Discrete pattern-specific damage mode

The SR activities increase where the damage is imposed and when the input is applied to that region of the network. To describe such concepts, a "damaging pattern" in the form of three vectors with different gradients of intensity is applied to the neuronal network (Figure 5A). This pattern is the same size as the neuronal network and only changes the ST factors. Importantly, this pattern does not alter the formation or the number of connections (Figure 5C). The value of ST = 1 is considered healthy, while any value lower than that indicates increasing damage (with values ranging from 0 to 1). In Figure 5A, the ST values of the three columns is gradually reduced from 1 to 0.7, 0.55, and 0.3 for columns (1), (2), and (3), respectively. Figure 5B shows the outline of these damaging patterns, plotted on top of the input samples. In experiment 2, the order and number of samples, and the current amplitude in the training and testing phases are identical to experiment 1.

The induced damage adversely affects the network by diminishing the efficacy of released neurotransmitters and gliotransmitters, consequently reducing the firing frequency of neurons (Figure 5D). In the first and second columns, the damage can be compensated through the SR mechanism. However, in the third column, the 70% damage hinders the release of sufficient neurotransmitters for initiating calcium waves, resulting in the absence of WM and SR activities (Figures 5D and 5E). The incorporation of the SR process enhances the firing frequency up to 100 Hz, representing a 30% improvement (Figure 5D, differences). Furthermore, it increases the robustness of recalled items from [0.66, 0.72, 0.77, 0.78] to [0.72, 0.9, 0.81, 0.84] for samples 0, 1, 2, and 3, respectively which is approximately 10–20% of improvement for each sample (Figures 5G and 5I).

The SR mechanism has the most significant impact on the second column, as it improves the consistency of neuronal firing, which is evident in the neuron membrane potential plots (Figures 5F and 5H) and the Video S1 (supplementary section). Another factor that facilitates the WM function is the propagation of Ca^{2+} between astrocytes, assisting in meeting the required Ca^{2+} conditions for both local and whole-cell activities of astrocytes (to be demonstrated in experiment 3). It is worth mentioning that during the training phase, there is minimal to no SR activities, as astrocytes have not yet generated enough Ca^{2+}. In conclusion, incorporating local astrocyte activities as the foundation of the SR mechanism enhances WM performance by improving the firing frequency up to 100 Hz in the damaged areas and increasing the correlation up to 20%.

Experiment 3 – Continuous pattern-specific damage mode

Experiment 2 demonstrated that the proposed SR algorithm only increases the SR activity in the impaired areas caused by a discrete damaging pattern. However, this damaging pattern is hypothetical and does not represent the continuous and random deterioration that characterizes most neurodegenerative diseases in the brain.[56] To address this limitation, experiment 3 evaluates the SR process for a continuous form of damage to the network where its intensity gradually increases up to 92% by moving toward the top right corner of the pattern (Figure 6B). Similar to experiment 2, this damaging pattern only affects the efficacy of the released neurotransmitters and the strength of synaptic connections.

By simulating this form of damage, this experiment aims to identify the SR threshold and the impact of intercellular Ca^{2+} propagation in the astrocytic network on both SR and WM mechanisms. In this way, the simulation setup needs to be different from the previous experiments. The idea is to have only two matched samples and compare the performance before and after the test phase (Figure 6A). Therefore, two diagonally striped non-overlapping patterns that can cover the whole network are designed (Figure 6C). The addition of the SR mechanism improves the firing frequency (in some areas) up to 100 Hz for each sample (Figure 6E). Due to the unique setup of this experiment, the total amount of improvement by the SR process on the whole network can be calculated by computing the summation of the "differences" (Figure 6F). Next, by comparing the damaging pattern (Figure 6B), total SR activities (Figure 6F), and the calcium concentration of the astrocytic network before the test phase (Figure 6D), the contribution of SR mechanism and intercellular astrocytic Ca^{2+} propagation can be identified. By performing this comparison four regions are identified (Figure 6G). First, the sections that could not encode information in the form of Ca^{2+} oscillations due to high damage intensity. Second, the regions that are healthy enough to have WM regardless of the SR process. Third, the parts that the SR mechanism is required to have a functional WM process. Fourth, the areas in which WM still depends on the SR mechanism, but the intercellular astrocytic Ca^{2+} propagation is the main contributing factor for the proper execution of the WM task. (Figure 6G).

Another improvement that the SR mechanism can provide is the concept of consistency in the frequency of firing which can be observed in the provided video in the supplementary material (Video S1). In the network without SR mechanism, the highlighted region 3 in Figure 6F exhibits a waveform action in its spiking responses. On the other hand, in the network with SR mechanism, this region exhibits a more stable neuronal firing in its WM intervals. This finding indicates that the SR process also improves the consistency of neuronal firing and WM performance. A similar behavior is also observed for sample "1" in experiment 2 which has been shown in the Video S1.

Experiment 4 – Analytic results for random damage mode

This experiment aims to simulate a developmental phase for a non-compact diffusive form of damage in order to identify the critical points of both WM and SR mechanisms. To model sporadic damage, random values for ST are assigned. Damage intensity is determined by reducing the distribution of ST values by 0.1 for every 5% increment in the damage (Figure 7A). For instance, 40% and 70% random damages are

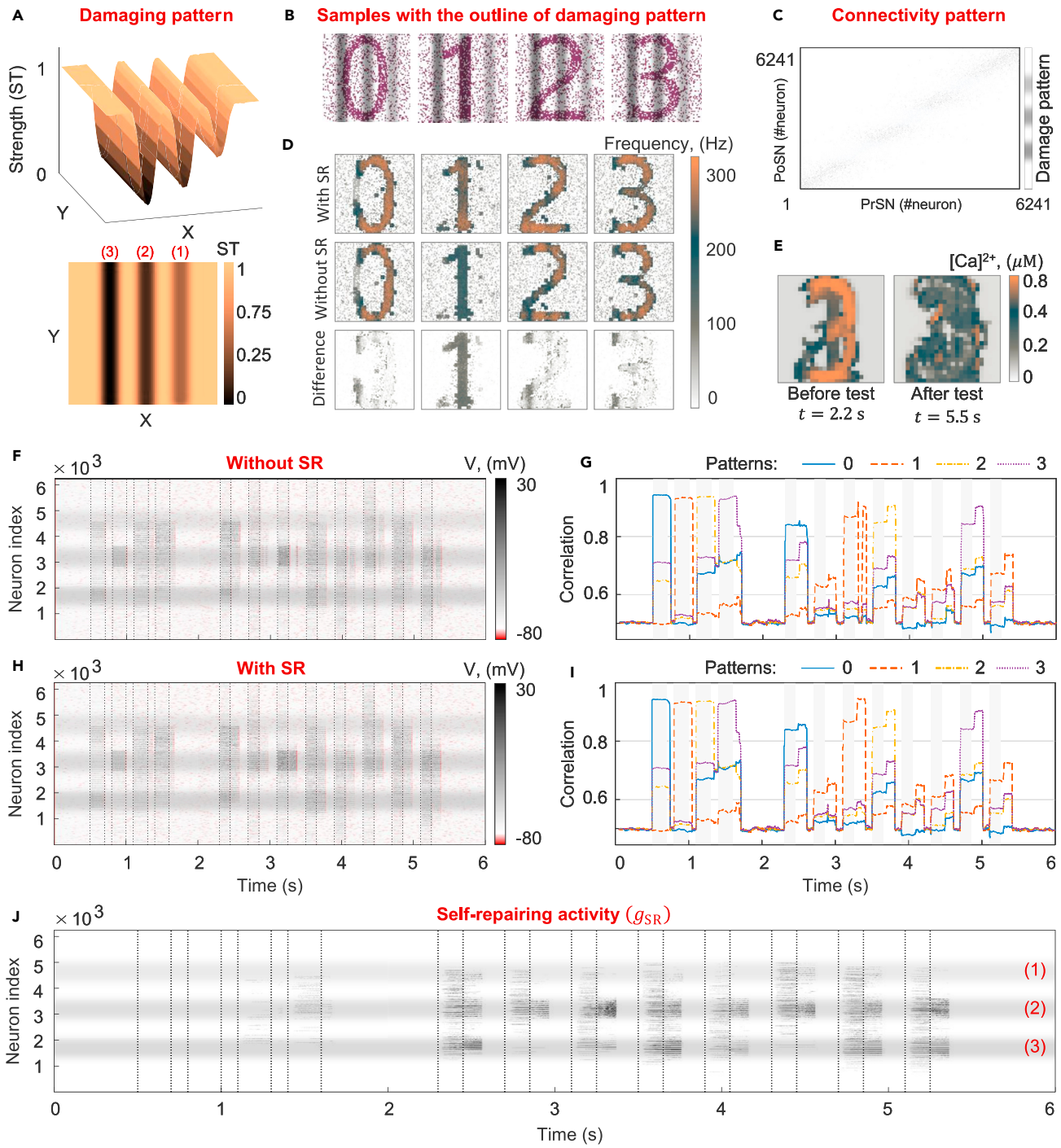

Figure 5. Experiment 2 – SR performance in a network with discrete regions of damage

(A) The damaging pattern in the form of three discrete columns is applied to the neuronal network, illustrated in 2D and 3D figures. The strength (ST) of the columns is reduced to 70%, 55%, and 30% from right to left, respectively.

(B) The outline of the damage is shown on top of the samples to identify where this damage alters the inputs.

(C) The connectivity patterns are illustrated.

(D) Snapshot of the frequency of firing indicates up to a 100 Hz improvement for the addition of the SR mechanism.

(E) snapshot of the astrocyte Ca^{2+} at 2.2 s indicates that the column with 70% damage prevents the release of adequate neurotransmitters for initiating calcium waves. Snapshot at 5.5 s shows the diffusion of Ca^{2+} in the astrocytic network which to some extent helps both the WM and SR processes.

(F and H) Neuronal membrane potential plots show that the addition of SR mechanism increases the consistency of firing.

(G and I) The calculated correlation with (i) and without (g) SR mechanism.

(J) The SR activity intensified the most in the impaired areas to compensate for the damage during WM intervals.

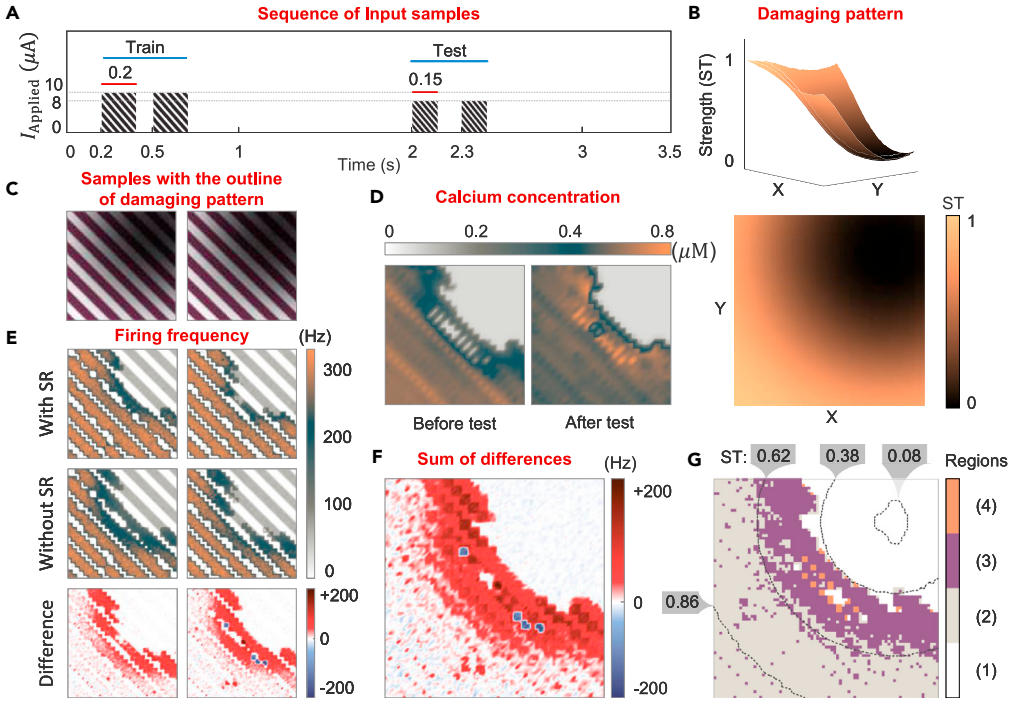

Figure 6. Experiment 3 – Evaluation of SR mechanism in a network with a continuous form of damage

(A) Timing of the samples in the train and test phases.

(B) Damage in the form of a continuous pattern is applied to the network. Strength (ST) continuously decreases by moving toward the top right corner of the network.

(C) To demonstrate the impact of the damaging pattern on the inputs, its outline is mapped on top of the samples.

(D) Calcium concentration in the astrocyte network before and after the test phases indicates the propagation of Ca^{2+} ions. Additionally, the area where no calcium was generated due to the high intensity of the damage is recognizable.

(E) Measuring the neural firing frequency illustrates a maximum of 100 Hz improvement for the network with SR mechanism.

(F) By taking the summation of the differences, the total SR activities can be identified. Negative values are the result of random noise in the system.

(G) Finally, by simultaneous consideration of the total SR activities (F), calcium concentration before the test (D), and contours of the applied damaging pattern (B), four regions are identified: (1) generated calcium is less than 0.15 μM, therefore, no WM activity occurs in these regions; (2) WM happens with or without the SR process since the summation of differences is less than 50 Hz; (3) SR process is a crucial factor for WM since the sum of differences is greater than 50 Hz. The SR mechanism has the most impact on regions with ST values between 0.38 and 0.62 in a network with continuous damage; (4) WM still depends on SR activity, but the calcium condition is satisfied due to the intercellular diffusion of Ca^{2+} through gap junctions. Indeed, in these regions, the Ca^{2+} concentration before the test phase is less than 0.15 μM, but the summation of differences is greater than 50 Hz, which can only occur by having WM activity.

characterized by a random selection of ST values between 0.2 and 1, and 0 to 0.6, respectively (Figures 8A and 8B). The number and sequence of samples in this experiment are those used in the experiment 1.

Since this experiment evaluates the performance of the SR mechanism on WM in 20 simulations with varying damage intensities, it is essential to quantify all utilized metrics in previous experiments, or normalize them based on the healthy condition. Robustness is determined by calculating the integral under the WM interval for each sample. The firing frequency is quantified by first computing the network firing rate within the 250 ms window of the test phase and then normalizing this value according to the value obtained for each sample in the healthy condition. This results in a proportion of the network firing rate based on the healthy condition. Total SR activities and bound neurotransmitters are calculated by the summation of their values over time and across the network for all neurons. Lastly, capacity should be defined, but specifying a general number for this metric is challenging, as the accuracy of recalled samples depends on the size, overlapping ratio, number, and sequence of matched and non-matched samples in the training and testing phases. However, in a controlled condition with constant parameters, improvement in capacity can be determined by preserving robustness at higher damage intensities due to the SR process, as opposed to the condition without the SR mechanism. By comparing the robustness with and without the SR mechanism in Figure 7B, it becomes evident that the network with SR capability can fully recall all matched samples up to 45% damage and partially recall some samples up to 60% synaptic impairment. In contrast, the robustness of the same network without SR mechanism start to fail from 35% damage and holds up to only 40% damage. This indicates that the addition of SR mechanism represents around a 20% improvement in the WM performance. Since damage is evenly distributed throughout the network in this experiment, the calculated value of robustness declines suddenly because either the entire neuronal network manages to produce strong activity to receive the whole-cell modulation of astrocytes for the WM task or the entire network fails to generate such activity.

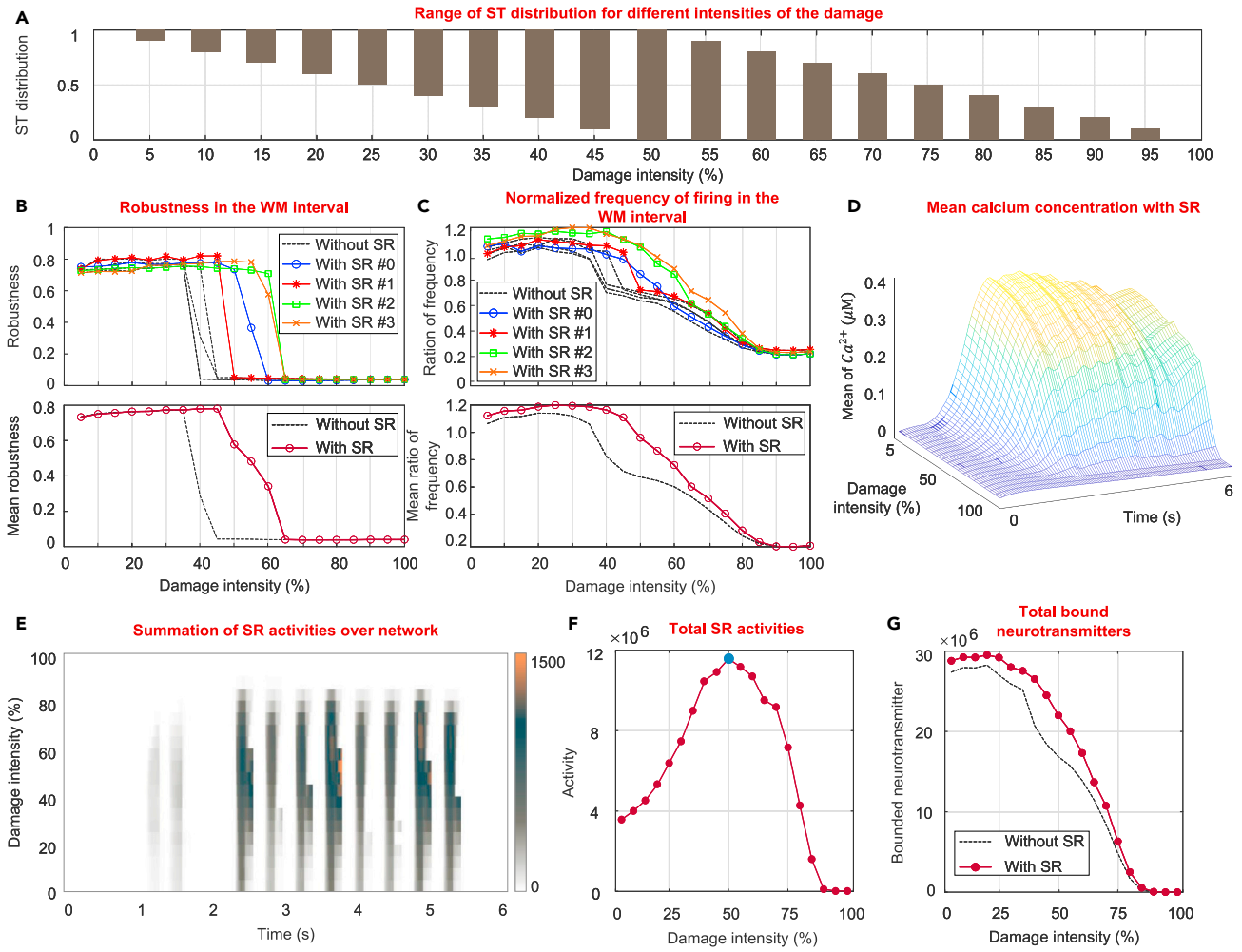

Figure 7. Experiment 4 –Results of applying random damage to the network

(A) Strength (ST) distribution for 20 simulations. The ST values change by 0.1 for every 5% increase in damage.

(B) The presence of the SR mechanism enhances robustness. Sample "1" is the first to fade due to its smaller size and overlapping ratio.

(C) Normalized firing frequency is computed by taking the summation of the firing frequency of the entire network during the 250 ms WM intervals and then normalizing it based on the healthy condition. As the damage intensity increases, this metric declines progressively.

(D) Intracellular Ca^{2+} concentration of astrocytes across the network for all 20 simulations is shown. As damage increases, the mean Ca^{2+} concentration decreases at a higher rate.

(E) Accumulated SR activities across the network is demonstrated. If WM fails, this activity also fails.

(F) Total SR activities exhibits a three times increase at the peak value compared to its initial level at the 50% damage. From this point on, although damage intensity increases, the SR activity starts to decline at a faster rate because of WM failure for matched samples.

(G) As damage increases, the total bound neurotransmitter begins to decrease.

As damage increases in the network equipped with the SR mechanism, the SR activities increase to compensate for the induced damage (Figure 7F), with its value peaking at 50% damage intensity. It is important to note that when WM starts to fail at 50% damage, the total bound neurotransmitters with astrocytes (Figure 7G) and the network firing frequency (Figure 7C) are already on a declining trend, leading to the reduced Ca^{2+} production in the astrocyte network (Figure 7D). This, in turn, leads to a failure in satisfying the Ca^{2+} condition of astrocytes for both whole-cell and local activities, causing a decrease in SR and WM activities.

Figure 8 examines the 40% and 50% random damage cases in more detail, since they are critical levels for failure of the WM mechanism. Considering the correlation plots for 40% random damage in Figure 8D, it is evident that WM is failed for the 2nd, 5th, and 6th samples in the test, as the correlation value is 0.5 or inconsistent in the WM interval. It is notable to mention that these three samples are all non-match samples while the data in Figure 7B are for matched samples. Furthermore, since SR activity depends on the WM activity and damage intensity, there is no SR activity during 0.1s of WM interval for these non-match samples with failed WM (Figure 8D). Looking at the correlation and SR activities of 50% random damage in Figure 8F, it becomes apparent that WM has failed for all non-match samples. The first matched sample

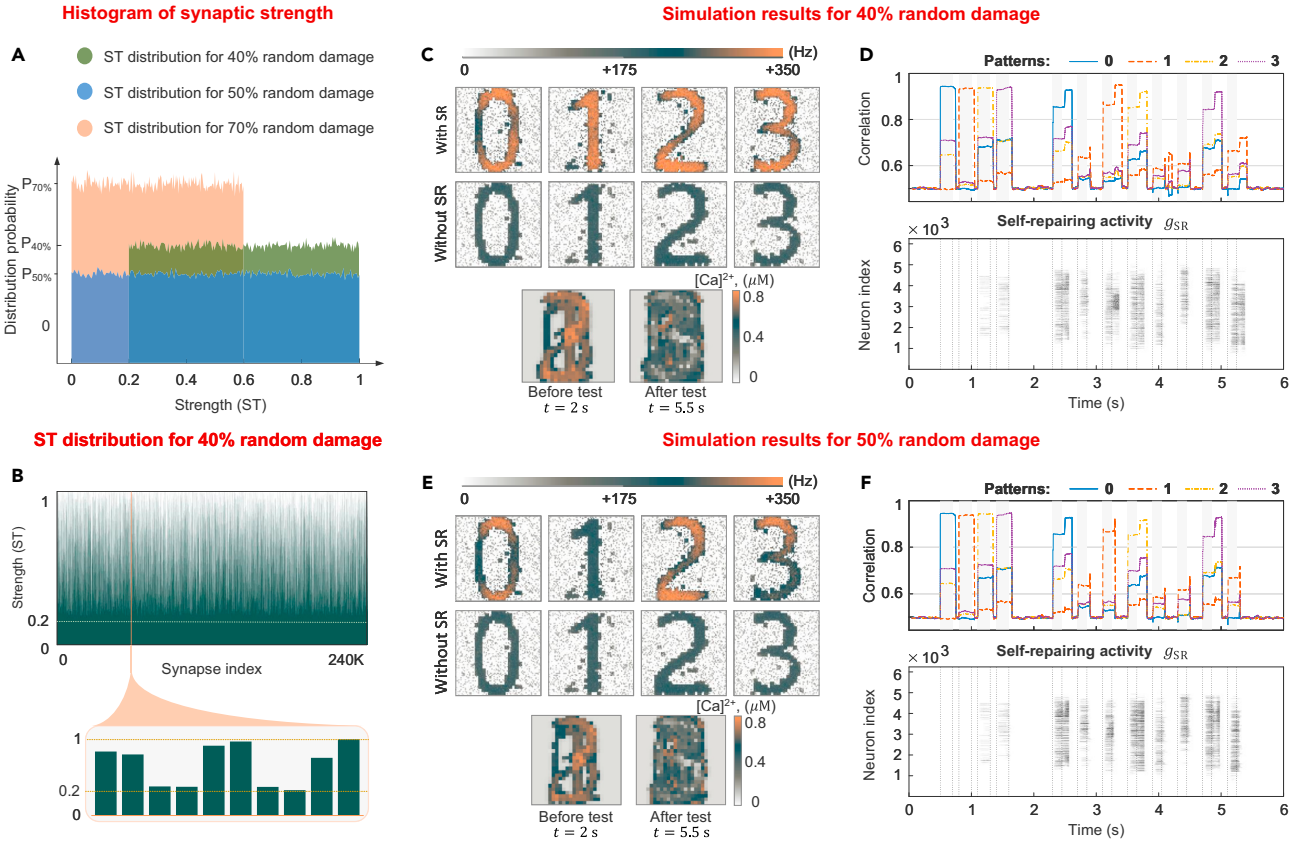

Figure 8. Further analysis for Experiment 4

(A) Histogram of strength (ST) for 40%, 50%, and 70% random damages are depicted. The distribution probability for each condition is calculated based on the given range for ST.

(B) The ST values for the 40% random damage is uniformly distributed between 0.2 and 1.

(C and E) Increases in damage impact not only the firing frequency but also the astrocytic Ca^{2+} propagation before the test phase. Firing frequency begins to decrease from areas with the minimum overlapping information.

(D and F) SR process depends on the WM activity. Comparing the SR activities plot with the correlation plot reveals that if WM fails, there is no SR signal in the extra 0.1 s interval where the neuronal network only fires due to astrocytes interaction. Additionally, as damage increases, WM initially fails for nonmatch samples and then for matched samples with the smallest size and minimum overlapping information, such as sample "1".

that fails WM is sample "1" because its size is relatively smaller and has the least overlapping area with the other samples (Figures 8E and 8F). Additionally, as the damage increases, the firing frequency starts to decrease from the parts with the least overlapping ratio (Figures 8C and 8E). In conclusion, considering simulations in Figure 8 and the data in Figure 7B, it can be deduced that the WM mechanism starts to fail first from non-match samples and then from matched samples with the smallest size and minimum overlapping ratio.

DISCUSSION

Over the past decades, the utilization of novel tools has yielded compelling evidence, highlighting the crucial involvement of dynamic interactions between astroglia and neurons in brain function.[73] Astrocytes are involved in major functions such as WM through their whole-cell modulation and can provide SR functionality through endocannabinoid pathways via their local activities.[14,27,60,74] This wealth of knowledge makes them suitable as therapeutic targets. To achieve this, a predictive simulation platform is required for a better understanding of neuron - astrocyte communication. However, none of the existing models in the literature utilize the supportive behavior of astrocytes alongside their other functionality. Most SNAN models focus on common astrocytic attributes in WM, such as multi-item WM,[15] WM with grayscale input,[16] situation-based WM,[19] and multiple forms of bistable gliotransmitter release[18] (Table 1). These previous works have some limitations, such as neglecting the released 2AG from neurons, considering either local or whole-cell activity from astrocytes, and not including the impact of SR mechanism on WM. This study aims to address the gap in understanding how astrocytes can facilitate WM function in a synaptically impaired network. It investigates neuronal-astrocytic interactions and proposes a large-scale SNAN that incorporates both local and whole-cell activities of astrocytes simultaneously. This approach demonstrates how astrocytes' SR mechanism can facilitate the WM function.

Table 1. Comparison with the previous implementation of WM and SR mechanisms in a spiking neuron-astrocyte network

	Network topology	Self-repairing	Working memory type	Implementation	Damage modes
This work	Neuron-astrocyte	BoF-based	Multi-item (logistics)	Software simulations	Automatic (random and pattern-specific)
Wade (2012)[30]	Neuron-astrocyte	PR-based	–	Software simulations	Manual (synaptic level)
Liu (2018)[75]	Neuron-astrocyte	PR-based	–	Digital FPGA	Manual (synaptic level)
Rahiminejad (2021)[76]	Neuron-astrocyte	PR-based	–	Analog CMOS	Manual (synaptic level)
Hong (2022)[77]	Neuron-astrocyte	PR-based	–	Memristive circuit	Manual (synaptic level)
Gordleeva (2021)[15]	Neuron-astrocyte	–	Multi-item (logistics)	Software simulations	–
Tsybina (2022)[16]	Neuron-astrocyte	–	Multi-Item (grayscale)	Software simulations	–
Gordleeva (2022)[19]	Neuron-astrocyte	–	Situation-based (logistics)	Software simulations	–
De Pittà (2022)[18]	Neuron-astrocyte	–	Bistable synaptic release	Software simulations	–

Previous implementations of the SR mechanism employed the transition probability (PR) of synapses to demonstrate this concept.[30,31,76–79] However, these studies were limited to use a probabilistic neuronal firing mechanism in a small network, and the entire process was anchored based on a constant modulation from astrocytes. Additionally, to test those models, the damage had to be manually imposed on some of the synapses. Furthermore, none of these models expanded the concept of SR mechanism to a large-scale SNAN. In the present study, a BoF-based SR algorithm was proposed for large-scale SNANs. The local activity of astrocytes in this algorithm, which leads to the SR process, can dynamically change based on the synaptic activities, enabling this model to be functional at the network level, operating in selective intervals of activities. Experimental data suggests that astrocyte-neuron interactions should be non-linear,[68] the dynamic local activities of astrocytes in this model is also a non-linear synapse-glia factor ($SoI_{Syn(N)}$). Another advantage of the presented model is its impairing algorithm. It can automatically damage the network either in a random manner or based on a "damaging pattern" through a series of ST factors. In contrast, previous PR-based SR models induced the damage manually by reducing a single factor of PR_0 for some of the synapses.[30] Compared to other WM models, the addition of the SR mechanism in the SNAN model increases the resilience of the WM function against the introduced synaptic damage. The astrocyte model utilized in this study, performs the local and whole-cell activities based on both the released glutamate and 2AG from neurons. This approach allows for a more accurate representation of the astrocyte-neuron interactions in an SNAN model.

To ensure that the introduced modifications in the model and the addition of the SR mechanism do not disrupt the WM functionality, the network was evaluated under healthy conditions in experiment 1. Simulation results suggested that the firing frequency and correlation of the test items in the modified network were similar to those in previous works without the proposed changes.[15] To further validate the effectiveness of the proposed SR algorithm, experiment 2 was conducted. Due to the network size, damaging a few synapses, as done in previous works, is insufficient to assess the functionality of the SR mechanism. Therefore, in experiment 2, the entire network was impaired with a damaging pattern consisting of three columns with varying intensities. This pattern was selected to allow for the visual identification of the damaged regions through analysis of the neuronal membrane potential and SR activities plots. As expected, the SR process got notably active in the damaged areas when those regions received an input stimulus. This is while the nearby astrocytes to the impaired parts demonstrated intercellular Ca^{2+} levels exceeding the threshold needed to initiate their local activities.

While experiment 2 effectively illustrated the characteristics of the SR mechanism, it did not represent a realistic condition in terms of damage formation. One of the characteristics of neurodegenerative diseases is the spongiform changes in specific brain areas.[56] The developmental phase, shape, and distribution of these changes vary depending on the region of the brain and type of the disease.[56] Typically, neurodegenerative diseases appear as heterogeneous dense cores and/or non-compact diffuse plaques.[56] To address these aspects, experiment 3 was designed to investigate the role of SR process in a dense core form of damage. In experiment 3, a different approach was taken in the stimulus setup compared to the other experiments. Two diagonally stripped non-overlapping patterns that could cover the entire network were selected as the input samples. This setup allowed for the realization of the SR threshold when a continuous form of damage was present. Simulation results indicated that the SR activities was most effective for ST values distributed between 0.38 and 0.62, enhancing the resilience of the WM functionality against damage by approximately 20% through the SR mechanism. Additionally, an algorithm was developed specifically for experiment 3 to identify which parts of the astrocytic network successfully perform the WM task through the propagation of the intercellular Ca^{2+} via gap junctions. This algorithm also identified those parts of the astrocytic network that are unable to encode information in the form of Ca^{2+} due to the high intensities of damage.

Experiment 4 aimed to replicate a developmental phase for non-compact random synaptic damage by reducing the distribution range for synaptic strength by 0.1 for every 5% increase in damage. Simulation results suggested that the addition of the SR mechanism increases the resilience of the network up to 60% synaptic impairment, which is a 20% improvement compared to the same network without SR capability. Furthermore, the findings revealed that the failure in the WM task first occurred with non-matched samples and then the matched samples with the smallest size and minimum overlapping ratio. These findings highlighted the importance of the size and overlapping information of the input samples in the consolidation of both WM and SR mechanisms. These results align with recent experimental findings where test

subjects exposed to visual inputs of different sizes demonstrated improved WM performance and learning processes as the input size increases.[80] Finally, it should be noted that previous studies on SR process could not conduct such detailed analyses due to their small size of implementation. Experiment 4 addressed this limitation and provided valuable insights into the impact of non-compact random synaptic damage on the SNAN's functionality.

Given the current debates and uncertainties surrounding the underlying mechanisms of gliotransmitter release from astrocytes, whether this signaling depends solely on the IP3R2 pathways or involves other processes,[81] the presented research foundation is based on the prevailing literature suggesting that the elevation of astrocytic Ca^{2+} fluxes is based on IP3R modulation due to the activation of mGluRs and GPCRs upon the secretion of neurotransmitters and endocannabinoids. Additionally, future works can incorporate other factors that contribute to global calcium signaling, such as extracellular calcium, ionotropic receptors, metabotropic receptors, and channels such as TRPA1 that could even account for 30–40% of Ca^{2+} elevation.[11] However, it is now evident that gliotransmission is a complex phenomenon involving various modes and signaling pathways. To gain a comprehensive understanding, it is necessary to employ advanced techniques and meticulously designed experiments for thorough investigation and elucidation.[81,82]

One of the main challenges in inducing damage to an SNAN is the consideration of the efficacy of the damage on the mathematical models. This problem arises from the lack of tight integration between different parts of the mathematical model. For example, most models implement their glutamate release equation in the synaptic clefts independent from the number of synaptic connections and the equation of the synaptic current in the neuronal model.[15] Although this type of modeling approximates healthy conditions fairly well, it does not accurately account for the effects of synaptic damage on the released glutamate. To address this issue, a new glutamate release model that takes the quantized number of activated synapses into account was proposed in this work, which is also in accordance with experimental evidence.[83] This work demonstrated how SR mechanism can improve the fault tolerance of the SNANs in the presence of synaptic damage. Additionally, the SR mechanism is generalized in the article to be easily adapted to other SNAN models such as De Pitta's model.[18]

Limitation of the study

One limitation of this study is the absence of synaptic plasticity in the presented SNAN model. It should be pointed out that, this exclusion does not undermine the fundamental premise of the research, which focuses on enhancing the WM mechanism through the SR process in a synaptically impaired network. However, this model can be further improved by including synaptic plasticity in future research.

Conclusion

To enable cognitive functions in both humans and animals, WM serves as a crucial mechanism for the momentary storage and management of data in goal-directed actions.[84–86] Glial cells have been identified as significant contributors to this process. Recent studies have revealed the pivotal role of astrocytes in synapse elimination, which can contribute to network dysfunction associated with neurodegeneration.[87] In addition, they are also involved with the facilitation of synaptic transmission by monitoring the released neurotransmitters and endocannabinoids in the tripartite synapses.[26] Through these signaling pathways, they can provide the SR mechanism. This study aimed to emphasize the importance of SR process in SNAN. The novelty of this work is the presentation of an SNAN with both WM and SR mechanisms. The WM was achieved through the whole-cell modulation of astrocytes, while SR process was derived from their local activity. Additionally, two depletion factors for both local and whole-cell activities of astrocytes were considered on their Ca^{2+} levels. To scale up the SR mechanism, the local activities of astrocytes were adapted based on the synaptic activities. To impose the damage, an algorithm was developed to automatically impair the synapses either randomly or based on a damaging pattern. To model the damage, a glutamate release equation was proposed that functions based on the synaptic activities. The significant findings from the conducted simulations demonstrated that the addition of SR mechanism increases the robustness of WM by approximately 20% in an impaired network by improving the consistency of the neuronal firing. Simulation results also suggested that intercellular astrocytic Ca^{2+} propagation via gap junctions, size of the input sample, and overlapping information contribute to the improvement of both WM and SR processes. Indeed, the presented research opens new frontiers in better understanding of the neuronal communication with astrocytes in synaptically impaired networks. Future work will focus on incorporating synaptic plasticity that functions with both WM and SR activities, allowing for the implementation of this model in Artificial Intelligence (AI) applications. Additionally, the performance of the model can be tested using different network connectivity patterns and various configurations of neuron-astrocyte interactions.

STAR★METHODS

Detailed methods are provided in the online version of this paper and include the following:

- KEY RESOURCES TABLE
- RESOURCE AVAILABILITY
  - Lead contact
  - Materials availability
  - Data and code availability
- METHOD DETAILS
  - Neuron model

- Neuron-astrocyte interaction
- Astrocyte model
- Astrocyte-neuron interaction
- Self-repairing mechanism (local interaction of astrocytes)
- Working memory mechanism (whole-cell interaction of astrocytes)
- Correlation

SUPPLEMENTAL INFORMATION

Supplemental information can be found online at https://doi.org/10.1016/j.isci.2023.108241.

ACKNOWLEDGMENTS

We would like to thank the esteemed reviewers for providing insightful comments.

Funding for this work was provided by the Human Frontier Science Program grant RGP0045/2022.

AUTHOR CONTRIBUTIONS

PN, AD and MA developed the computational model and experiments. MA and HP did the conception and design. All authors edited the article and accepted the final version.

DECLARATION OF INTERESTS

The authors declare no competing interests.

Received: March 8, 2023
Revised: August 23, 2023
Accepted: October 15, 2023
Published: October 21, 2023

REFERENCES

1. Kugler, E.C., Greenwood, J., and MacDonald, R.B. (2021). The "Neuro-Glial-Vascular" Unit: The Role of Glia in Neurovascular Unit Formation and Dysfunction. Front. Cell Dev. Biol. *9*, 732820. https://doi.org/10.3389/fcell.2021.732820.
2. Akdemir, E.S., Huang, A.Y.-S., and Deneen, B. (2020). Astrocytogenesis: where, when, and how. F1000Res. *9*. Faculty Rev-233. https://doi.org/10.12688/f1000research.22405.1.
3. Slezak, M., and Pfrieger, F.W. (2003). New roles for astrocytes: regulation of CNS synaptogenesis. Trends Neurosci. *26*, 531–535.
4. Kettenmann, H., and Ransom, B.R. (2012). Neuroglia (Oxford University Press).
5. Khakh, B.S., and Sofroniew, M.V. (2015). Diversity of astrocyte functions and phenotypes in neural circuits. Nat. Neurosci. *18*, 942–952. https://doi.org/10.1038/nn.4043.
6. Henneberger, C., and Rusakov, D.A. (2012). Monitoring local synaptic activity with astrocytic patch pipettes. Nat. Protoc. *7*, 2171–2179. https://doi.org/10.1038/nprot.2012.140.
7. Semyanov, A., Henneberger, C., and Agarwal, A. (2020). Making sense of astrocytic calcium signals — from acquisition to interpretation. Nat. Rev. Neurosci. *21*, 551–564. https://doi.org/10.1038/s41583-020-0361-8.
8. Tong, X., Shigetomi, E., Looger, L.L., and Khakh, B.S. (2013). Genetically Encoded Calcium Indicators and Astrocyte Calcium Microdomains. Neuroscientist *19*, 274–291. https://doi.org/10.1177/1073858412468794.
9. Shigetomi, E., Kracun, S., and Khakh, B.S. (2010). Monitoring astrocyte calcium microdomains with improved membrane targeted GCaMP reporters. Neuron Glia Biol. *6*, 183–191. https://doi.org/10.1017/S1740925X10000219.
10. Shigetomi, E., Tong, X., Kwan, K.Y., Corey, D.P., and Khakh, B.S. (2011). TRPA1 channels regulate astrocyte resting calcium and inhibitory synapse efficacy through GAT-3. Nat. Neurosci. *15*, 70–80. https://doi.org/10.1038/nn.3000.
11. Srinivasan, R., Huang, B.S., Venugopal, S., Johnston, A.D., Chai, H., Zeng, H., Golshani, P., and Khakh, B.S. (2015). Ca(2+) signaling in astrocytes from Ip3r2(-/-) mice in brain slices and during startle responses *in vivo*. Nat. Neurosci. *18*, 708–717. https://doi.org/10.1038/nn.4001.
12. Guerra-Gomes, S., Sousa, N., Pinto, L., and Oliveira, J.F. (2017). Functional Roles of Astrocyte Calcium Elevations: From Synapses to Behavior. Front. Cell. Neurosci. *11*, 427.
13. Dingledine, R., Borges, K., Bowie, D., and Traynelis, S.F. (1999). The glutamate receptor ion channels. Pharmacol. Rev. *51*, 7–61.
14. Bernal-Chico, A., Tepavcevic, V., Manterola, A., Utrilla, C., Matute, C., and Mato, S. (2023). Endocannabinoid signaling in brain diseases: Emerging relevance of glial cells. Glia *71*, 103–126. https://doi.org/10.1002/glia.24172.
15. Gordleeva, S.Y., Tsybina, Y.A., Krivonosov, M.I., Ivanchenko, M.V., Zaikin, A.A., Kazantsev, V.B., and Gorban, A.N. (2021). Modeling Working Memory in a Spiking Neuron Network Accompanied by Astrocytes. Front. Cell. Neurosci. *15*, 631485. https://doi.org/10.3389/fncel.2021.631485.
16. Tsybina, Y., Kastalskiy, I., Krivonosov, M., Zaikin, A., Kazantsev, V., Gorban, A.N., and Gordleeva, S. (2022). Astrocytes mediate analogous memory in a multi-layer neuron–astrocyte network. Neural Comput. Appl. *34*, 9147–9160. https://doi.org/10.1007/s00521-022-06936-9.
17. Tsybina, Y., Gordleeva, S., Krivonosov, M., Kastalskiy, I., Zaikin, A., and Gorban, A. (2021). Modelling working memory in neuron-astrocyte network. In 2021 International Joint Conference on Neural Networks (IJCNN) (IEEE), pp. 1–6. https://doi.org/10.1109/IJCNN52387.2021.9533307.
18. De Pittà, M., and Brunel, N. (2022). Multiple forms of working memory emerge from synapse–astrocyte interactions in a neuron–glia network model. Proc. Natl. Acad. Sci. USA *119*, e2207912119. https://doi.org/10.1073/pnas.2207912119.
19. Gordleeva, S., Tsybina, Y.A., Krivonosov, M.I., Tyukin, I.Y., Kazantsev, V.B., Zaikin, A.A., and Gorban, A.N. (2022). Situation-based memory in spiking neuron-astrocyte network. Preprint at arXiv. https://doi.org/10.48550/arXiv.2202.07218.
20. Araque, A., Parpura, V., Sanzgiri, R.P., and Haydon, P.G. (1999). Tripartite synapses: glia, the unacknowledged partner. Trends Neurosci. *22*, 208–215. https://doi.org/10.1016/s0166-2236(98)01349-6.
21. Santello, M., Calì, C., and Bezzi, P. (2012). Gliotransmission and the tripartite synapse. Adv. Exp. Med. Biol. *970*, 307–331. https://doi.org/10.1007/978-3-7091-0932-8_14.
22. Perea, G., Navarrete, M., and Araque, A. (2009). Tripartite synapses: astrocytes process and control synaptic information. Trends

Neurosci. *32*, 421–431. https://doi.org/10.1016/j.tins.2009.05.001.
23. A. Volterra, P.J. Magistretti, and P.G. Haydon, eds. (2002). The tripartite synapse: glia in synaptic transmission (Oxford University Press).
24. Hille, B. (1978). Ionic channels in excitable membranes. Current problems and biophysical approaches. Biophys. J. *22*, 283–294. https://doi.org/10.1016/S0006-3495(78)85489-7.
25. Perea, G., and Araque, A. (2005). Glial calcium signaling and neuron–glia communication. Cell Calcium *38*, 375–382.
26. Navarrete, M., and Araque, A. (2010). Endocannabinoids Potentiate Synaptic Transmission through Stimulation of Astrocytes. Neuron *68*, 113–126. https://doi.org/10.1016/j.neuron.2010.08.043.
27. Alger, B.E. (2002). Retrograde signaling in the regulation of synaptic transmission: focus on endocannabinoids. Prog. Neurobiol. *68*, 247–286. https://doi.org/10.1016/S0301-0082(02)00080-1.
28. Navarrete, M., and Araque, A. (2008). Endocannabinoids Mediate Neuron-Astrocyte Communication. Neuron *57*, 883–893. https://doi.org/10.1016/j.neuron.2008.01.029.
29. Navarrete, M., Díez, A., and Araque, A. (2014). Astrocytes in endocannabinoid signalling. Phil. Trans. R. Soc. B *369*, 20130599. https://doi.org/10.1098/rstb.2013.0599.
30. Wade, J., McDaid, L., Harkin, J., Crunelli, V., and Kelso, S. (2012). Self-repair in a bidirectionally coupled astrocyte-neuron (AN) system based on retrograde signaling. Front. Comput. Neurosci. *6*, 76. https://doi.org/10.3389/fncom.2012.00076.
31. Liu, J., McDaid, L.J., Harkin, J., Wade, J.J., Karim, S., Johnson, A.P., Millard, A.G., Halliday, D.M., Tyrrell, A.M., and Timmis, J. (2017). Self-repairing Learning Rule for Spiking Astrocyte-Neuron Networks. In Neural Information Processing Lecture Notes in Computer Science, D. Liu, S. Xie, Y. Li, D. Zhao, and E.-S.M. El-Alfy, eds. (Springer International Publishing), pp. 384–392. https://doi.org/10.1007/978-3-319-70136-3_41.
32. Baldwin, K.T., and Eroglu, C. (2017). Molecular Mechanisms of Astrocyte-Induced Synaptogenesis. Curr. Opin. Neurobiol. *45*, 113–120. https://doi.org/10.1016/j.conb.2017.05.006.
33. Dallérac, G., Zapata, J., and Rouach, N. (2018). Versatile control of synaptic circuits by astrocytes: where, when and how? Nat. Rev. Neurosci. *19*, 729–743. https://doi.org/10.1038/s41583-018-0080-6.
34. Cowan, N. (2014). Working Memory Underpins Cognitive Development, Learning, and Education. Educ. Psychol. Rev. *26*, 197–223. https://doi.org/10.1007/s10648-013-9246-y.
35. Bakin, J.S., Weinberger, N.M., Sharma, J., Perea, G., Petravicz, J., Le, C., and Sur, M. (1996). Induction of a physiological memory in the cerebral cortex by stimulation of the nucleus basalis. Proc. Natl. Acad. Sci. USA *93*, 11219–11224. https://doi.org/10.1073/pnas.93.20.11219.
36. Schummers, J., Yu, H., and Sur, M. (2008). Tuned Responses of Astrocytes and Their Influence on Hemodynamic Signals in the Visual Cortex. Science *320*, 1638–1643. https://doi.org/10.1126/science.1156120.
37. Wasmuht, D.F., Spaak, E., Buschman, T.J., Miller, E.K., and Stokes, M.G. (2018). Intrinsic neuronal dynamics predict distinct functional roles during working memory. Nat. Commun. *9*, 3499. https://doi.org/10.1038/s41467-018-05961-4.
38. Stobart, J.L., Ferrari, K.D., Barrett, M.J.P., Glück, C., Stobart, M.J., Zuend, M., and Weber, B. (2018). Cortical circuit activity evokes rapid astrocyte calcium signals on a similar timescale to neurons. Neuron *98*, 726–735.e4. https://doi.org/10.1016/j.neuron.2018.03.050.
39. Wang, X., Lou, N., Xu, Q., Tian, G.-F., Peng, W.G., Han, X., Kang, J., Takano, T., and Nedergaard, M. (2006). Astrocytic Ca2+ signaling evoked by sensory stimulation *in vivo*. Nat. Neurosci. *9*, 816–823. https://doi.org/10.1038/nn1703.
40. Buzsaki, G., Bickford, R.G., Ponomareff, G., Thal, L.J., Mandel, R., Gage, F.H., and Hirase, H. (1988). Astrocyte calcium signaling transforms cholinergic modulation to cortical plasticity In vivo. J. Neurosci. *8*, 4007–4026. 20026212.
41. Durkee, C.A., and Araque, A. (2019). Diversity and Specificity of Astrocyte–neuron Communication. Neuroscience *396*, 73–78. https://doi.org/10.1016/j.neuroscience.2018.11.010.
42. Santello, M., Toni, N., and Volterra, A. (2019). Astrocyte function from information processing to cognition and cognitive impairment. Nat. Neurosci. *22*, 154–166. https://doi.org/10.1038/s41593-018-0325-8.
43. Perea, G., Yang, A., Boyden, E.S., and Sur, M. (2014). Optogenetic astrocyte activation modulates response selectivity of visual cortex neurons *in vivo*. Nat. Commun. *5*, 3262. https://doi.org/10.1038/ncomms4262.
44. Jourdain, P., Bergersen, L.H., Bhaukaurally, K., Bezzi, P., Santello, M., Domercq, M., Matute, C., Tonello, F., Gundersen, V., and Volterra, A. (2007). Glutamate exocytosis from astrocytes controls synaptic strength. Nat. Neurosci. *10*, 331–339. https://doi.org/10.1038/nn1849.
45. Navarrete, M., Perea, G., Fernandez de Sevilla, D., Gómez-Gonzalo, M., Núñez, A., Martín, E.D., and Araque, A. (2012). Astrocytes Mediate In Vivo Cholinergic-Induced Synaptic Plasticity. PLoS Biol. *10*, e1001259. https://doi.org/10.1371/journal.pbio.1001259.
46. Perea, G., and Araque, A. (2007). Astrocytes Potentiate Transmitter Release at Single Hippocampal Synapses. Science *317*, 1083–1086. https://doi.org/10.1126/science.1144640.
47. Stellwagen, D., and Malenka, R.C. (2006). Synaptic scaling mediated by glial TNF-α. Nature *440*, 1054–1059. https://doi.org/10.1038/nature04671.
48. Solovyeva, K.P., Karandashev, I.M., Zhavoronkov, A., and Dunin-Barkowski, W.L. (2015). Models of Innate Neural Attractors and Their Applications for Neural Information Processing. Front. Syst. Neurosci. *9*, 178. https://doi.org/10.3389/fnsys.2015.00178.
49. Lobo, J.L., Del Ser, J., Bifet, A., and Kasabov, N. (2020). Spiking Neural Networks and online learning: An overview and perspectives. Neural Network. *121*, 88–100. https://doi.org/10.1016/j.neunet.2019.09.004.
50. Zenke, F., Agnes, E.J., and Gerstner, W. (2015). Diverse synaptic plasticity mechanisms orchestrated to form and retrieve memories in spiking neural networks. Nat. Commun. *6*, 6922. https://doi.org/10.1038/ncomms7922.
51. Hopfield, J.J. (1982). Neural networks and physical systems with emergent collective computational abilities. Proc. Natl. Acad. Sci. USA *79*, 2554–2558. https://doi.org/10.1073/pnas.79.8.2554.
52. Goldman, M.S. (2009). Memory without Feedback in a Neural Network. Neuron *61*, 621–634. https://doi.org/10.1016/j.neuron.2008.12.012.
53. Lobov, S.A., Zharinov, A.I., Makarov, V.A., and Kazantsev, V.B. (2021). Spatial Memory in a Spiking Neural Network with Robot Embodiment. Sensors *21*, 2678. https://doi.org/10.3390/s21082678.
54. Tsodyks, M.V., and Markram, H. (1997). The neural code between neocortical pyramidal neurons depends on neurotransmitter release probability. Proc. Natl. Acad. Sci. USA *94*, 719–723. https://doi.org/10.1073/pnas.94.2.719.
55. De Pittà, M., Volman, V., Berry, H., and Ben-Jacob, E. (2011). A Tale of Two Stories: Astrocyte Regulation of Synaptic Depression and Facilitation. PLoS Comput. Biol. *7*, e1002293. https://doi.org/10.1371/journal.pcbi.1002293.
56. Dugger, B.N., and Dickson, D.W. (2017). Pathology of Neurodegenerative Diseases. Cold Spring Harbor Perspect. Biol. *9*, a028035. https://doi.org/10.1101/cshperspect.a028035.
57. Oberheim, N.A., Wang, X., Goldman, S., and Nedergaard, M. (2006). Astrocytic complexity distinguishes the human brain. Trends Neurosci. *29*, 547–553. https://doi.org/10.1016/j.tins.2006.08.004.
58. Oberheim, N.A., Takano, T., Han, X., He, W., Lin, J.H.C., Wang, F., Xu, Q., Wyatt, J.D., Pilcher, W., Ojemann, J.G., et al. (2009). Uniquely Hominid Features of Adult Human Astrocytes. J. Neurosci. *29*, 3276–3287. https://doi.org/10.1523/JNEUROSCI.4707-08.2009.
59. Halassa, M.M., Fellin, T., Takano, H., Dong, J.-H., and Haydon, P.G. (2007). Synaptic Islands Defined by the Territory of a Single Astrocyte. J. Neurosci. *27*, 6473–6477. https://doi.org/10.1523/JNEUROSCI.1419-07.2007.
60. Baraibar A.M., Belisle L., Marsicano G., Matute C., Mato S., Araque A., Kofuji P. Spatial Organization of Neuron-Astrocyte Interactions in the Somatosensory Cortex. Cerebral Cortex. *33*, 4498–4511. https://doi.org/10.1093/cercor/bhac357.
61. Giaume, C., Koulakoff, A., Roux, L., Holcman, D., and Rouach, N. (2010). Astroglial networks: a step further in neuroglial and gliovascular interactions. Nat. Rev. Neurosci. *11*, 87–99.
62. Nagy, J.I., and Rash, J.E. (2000). Connexins and gap junctions of astrocytes and oligodendrocytes in the CNS. Brain Res. Rev. *32*, 29–44. https://doi.org/10.1016/S0165-0173(99)00066-1.
63. Yamamoto, T., Ochalski, A., Hertzberg, E.L., and Nagy, J.I. (1990). On the organization of astrocytic gap junctions in rat brain as suggested by LM and EM immunohistochemistry of connexin43 expression. J. Comp. Neurol. *302*, 853–883. https://doi.org/10.1002/cne.903020414.
64. Parpura, V., and Haydon, P.G. (2000). Physiological astrocytic calcium levels stimulate glutamate release to modulate adjacent neurons. Proc. Natl. Acad. Sci. USA *97*, 8629–8634.
65. Agulhon, C., Petravicz, J., McMullen, A.B., Sweger, E.J., Minton, S.K., Taves, S.R.,

Casper, K.B., Fiacco, T.A., and McCarthy, K.D. (2008). What Is the Role of Astrocyte Calcium in Neurophysiology? Neuron *59*, 932–946. https://doi.org/10.1016/j.neuron.2008.09.004.

66. Fellin, T., Pascual, O., Gobbo, S., Pozzan, T., Haydon, P.G., and Carmignoto, G. (2004). Neuronal Synchrony Mediated by Astrocytic Glutamate through Activation of Extrasynaptic NMDA Receptors. Neuron *43*, 729–743. https://doi.org/10.1016/j.neuron.2004.08.011.
67. Miller, E.K., Erickson, C.A., and Desimone, R. (1996). Neural Mechanisms of Visual Working Memory in Prefrontal Cortex of the Macaque. J. Neurosci. *16*, 5154–5167. https://doi.org/10.1523/JNEUROSCI.16-16-05154.1996.
68. Perea, G., and Araque, A. (2005). Properties of synaptically evoked astrocyte calcium signal reveal synaptic information processing by astrocytes. J. Neurosci. *25*, 2192–2203.
69. Constantinidis, C., Funahashi, S., Lee, D., Murray, J.D., Qi, X.-L., Wang, M., and Arnsten, A.F.T. (2018). Persistent Spiking Activity Underlies Working Memory. J. Neurosci. *38*, 7020–7028. https://doi.org/10.1523/JNEUROSCI.2486-17.2018.
70. Sreenivasan, K.K., and D'Esposito, M. (2019). The what, where and how of delay activity. Nat. Rev. Neurosci. *20*, 466–481. https://doi.org/10.1038/s41583-019-0176-7.
71. Bindocci, E., Savtchouk, I., Liaudet, N., Becker, D., Carriero, G., and Volterra, A. (2017). Three-dimensional Ca2+ imaging advances understanding of astrocyte biology. Science *356*, eaai8185. https://doi.org/10.1126/science.aai8185.
72. Araque, A., Carmignoto, G., Haydon, P.G., Oliet, S.H.R., Robitaille, R., and Volterra, A. (2014). Gliotransmitters travel in time and space. Neuron *81*, 728–739.
73. Lia, A., Henriques, V.J., Zonta, M., Chiavegato, A., Carmignoto, G., Gómez-Gonzalo, M., and Losi, G. (2021). Calcium Signals in Astrocyte Microdomains, a Decade of Great Advances. Front. Cell. Neurosci. *15*, 673433. https://doi.org/10.3389/fncel.2021.673433.
74. Hegyi, Z., Oláh, T., Kőszeghy, Á., Piscitelli, F., Holló, K., Pál, B., Csernoch, L., Di Marzo, V., and Antal, M. (2018). CB1 receptor activation induces intracellular Ca2+ mobilization and 2-arachidonoylglycerol release in rodent spinal cord astrocytes. Sci. Rep. *8*, 10562. https://doi.org/10.1038/s41598-018-28763-6.
75. Liu, J., Harkin, J., Maguire, L.P., McDaid, L.J., and Wade, J.J. (2018). SPANNER: A Self-Repairing Spiking Neural Network Hardware Architecture. IEEE Transact. Neural Networks Learn. Syst. *29*, 1287–1300. https://doi.org/10.1109/TNNLS.2017.2673021.
76. Rahiminejad, E., Azad, F., Parvizi-Fard, A., Amiri, M., and Linares-Barranco, B. (2022). A Neuromorphic CMOS Circuit With Self-Repairing Capability. IEEE Transact. Neural Networks Learn. Syst. *33*, 2246–2258. https://doi.org/10.1109/TNNLS.2020.3045019.
77. Hong, Q., Chen, H., Sun, J., and Wang, C. (2022). Memristive Circuit Implementation of a Self-Repairing Network Based on Biological Astrocytes in Robot Application. IEEE Transact. Neural Networks Learn. Syst. *33*, 2106–2120. https://doi.org/10.1109/TNNLS.2020.3041624.
78. Veisi, N., Karimi, G., Ranjbar, M., and Abbott, D. (2022). Role of astrocytes in the self-repairing characteristics of analog neural networks. Neurocomputing *496*, 158–165. https://doi.org/10.1016/j.neucom.2022.01.077.
79. Azad, F., Shalchian, M., and Amiri, M. (2018). Circuit modelling of 2-AG indirect pathway via astrocyte as a catalyst for synaptic self repair. Analog Integr. Circuits Signal Process. *95*, 127–139. https://doi.org/10.1007/s10470-018-1106-8.
80. Masarwa, S., Kreichman, O., and Gilaie-Dotan, S. (2022). Larger images are better remembered during naturalistic encoding. Proc. Natl. Acad. Sci. USA *119*, e2119614119. https://doi.org/10.1073/pnas.2119614119.
81. Savtchouk, I., and Volterra, A. (2018). Gliotransmission: Beyond Black-and-White. J. Neurosci. *38*, 14–25. https://doi.org/10.1523/JNEUROSCI.0017-17.2017.
82. Petravicz, J., Boyt, K.M., and McCarthy, K.D. (2014). Astrocyte IP3R2-dependent Ca2+ signaling is not a major modulator of neuronal pathways governing behavior. Front. Behav. Neurosci. *8*, 384.
83. del Castillo, J., and Katz, B. (1954). Quantal components of the end-plate potential. J. Physiol. *124*, 560–573. https://doi.org/10.1113/jphysiol.1954.sp005129.
84. Baddeley, A. (1992). Working Memory. Science *255*, 556–559. https://doi.org/10.1126/science.1736359.
85. Baddeley, A. (2012). Working Memory: Theories, Models, and Controversies. Annu. Rev. Psychol. *63*, 1–29. https://doi.org/10.1146/annurev-psych-120710-100422.
86. Conway, A.R.A., Kane, M.J., and Engle, R.W. (2003). Working memory capacity and its relation to general intelligence. Trends Cognit. Sci. *7*, 547–552. https://doi.org/10.1016/j.tics.2003.10.005.
87. Henstridge, C.M., Tzioras, M., and Paolicelli, R.C. (2019). Glial Contribution to Excitatory and Inhibitory Synapse Loss in Neurodegeneration. Front. Cell. Neurosci. *13*, 63. https://doi.org/10.3389/fncel.2019.00063.
88. Izhikevich, E.M. (2003). Simple model of spiking neurons. IEEE Trans. Neural Network. *14*, 1569–1572. https://doi.org/10.1109/TNN.2003.820440.
89. Esir, P.M., Gordleeva, S.Y., Simonov, A.Y., Pisarchik, A.N., and Kazantsev, V.B. (2018). Conduction delays can enhance formation of up and down states in spiking neuronal networks. Phys. Rev. E *98*, 052401. https://doi.org/10.1103/PhysRevE.98.052401.
90. Kazantsev, V.B., and Asatryan, S.Y. (2011). Bistability induces episodic spike communication by inhibitory neurons in neuronal networks. Phys. Rev. E *84*, 031913. https://doi.org/10.1103/PhysRevE.84.031913.
91. Fatt, P., and Katz, B. (1952). Spontaneous subthreshold activity at motor nerve endings. J. Physiol. *117*, 109–128.
92. Nadkarni, S., and Jung, P. (2003). Spontaneous Oscillations of Dressed Neurons: A New Mechanism for Epilepsy? Phys. Rev. Lett. *91*, 268101. https://doi.org/10.1103/PhysRevLett.91.268101.
93. Ullah, G., Jung, P., and Cornell-Bell, A.H. (2006). Anti-phase calcium oscillations in astrocytes via inositol (1, 4, 5)-trisphosphate regeneration. Cell Calcium *39*, 197–208. https://doi.org/10.1016/j.ceca.2005.10.009.
94. Li, Y.-X., and Rinzel, J. (1994). Equations for InsP3 Receptor-mediated [Ca2+]i Oscillations Derived from a Detailed Kinetic Model: A Hodgkin-Huxley Like Formalism. J. Theor. Biol. *166*, 461–473. https://doi.org/10.1006/jtbi.1994.1041.
95. Nimmerjahn, A., Kirchhoff, F., Kerr, J.N.D., and Helmchen, F. (2004). Sulforhodamine 101 as a specific marker of astroglia in the neocortex *in vivo*. Nat. Methods *1*, 31–37. https://doi.org/10.1038/nmeth706.
96. Chen, N., Sugihara, H., Sharma, J., Perea, G., Petravicz, J., Le, C., and Sur, M. (2012). Nucleus basalis-enabled stimulus-specific plasticity in the visual cortex is mediated by astrocytes. Proc. Natl. Acad. Sci. USA *109*, E2832–E2841. https://doi.org/10.1073/pnas.1206557109.

STAR★METHODS

KEY RESOURCES TABLE

REAGENT or RESOURCE	SOURCE	IDENTIFIER
Software and algorithms		
MATLAB	MathWorks	https://www.mathworks.com/
Adobe illustrator	Adobe	https://www.adobe.com/products/illustrator.html
Adobe photoshop	Adobe	https://www.adobe.com/products/photoshop.html
Microsoft Visio	Microsoft	https://www.office.com/
BioRender	BioRender	https://www.biorender.com/
Working memory code	GitHub	https://github.com/altergot/neuro-astro-network
Self-repairing algorithm	IEEE	https://ieeexplore.ieee.org/document/6033638
Working memory with self-repairing code	This work	https://github.com/Research-lab-KUMS/working-memory-with-self-repairing

RESOURCE AVAILABILITY

Lead contact

Dr. Mahmood Amiri
Medical Technology Research Center, Institute of Health Technology, Kermanshah University of Medical Sciences, Kermanshah, Iran
Email: Ma_amiri_bme@yahoo.com

Materials availability

This study did not generate new unique reagents.

Data and code availability

- Data: No new data were generated.
- Code: Original code has been deposited at https://github.com/Research-lab-KUMS/working-memory-with-self-repairing.
- Any additional information is available from the lead contact upon request.

METHOD DETAILS

The equations of the model are presented in their order of execution. First, input and neuronal networks are presented, then neuron-astrocyte interaction. Next, the astrocyte model, and finally the astrocyte-neuron interactions are presented. In the last section, the local activity of astrocytes describes the mathematical model of the proposed BoF-based SR algorithm and the whole-cell astrocyte activity depicts the WM model. The values of the constant parameters are provided in the Tables S1–S4.

Neuron model

The Izhikevich neuronal model is used[88] as follows:

$$\frac{dV^{(i,j)}}{dt} = 0.04V^{(i,j)^{(2)}} + 5V^{(i,j)} - U^{(i,j)} + 140 + I_{Sum}^{(i,j)}$$

$$\frac{dU^{(i,j)}}{dt} = a\left(bV^{(i,j)} - U^{(i,j)}\right)$$

$$I_{Sum}^{(i,j)} = I_{App}^{(i,j)} + I_{Syn}^{(i,j)} + ST2^{(i,j)}\left(I_{Noise}^{(i,j)}\right) \quad \text{(Equation 1)}$$

Voltage values will reset with the auxiliary after-spike resetting:

$$\text{if } V^{(i,j)} \geq 30\text{mV, then } \begin{cases} V^{(i,j)} \leftarrow c \\ U^{(i,j)} \leftarrow U^{(i,j)} + d \end{cases} \quad \text{(Equation 2)}$$

where superscripts $i, j \in \{1, \ldots, 79\}$ represent the coordinates of neurons on a square grid, the membrane potential V (which is V_{Post} in the network) is calculated in mV with the timescale ms. The damage is introduced by ST (strength) variables. In default mode (healthy condition) the ST values are set to one. To induce damage, these values are modified to a value between 0 to 1. Regardless of the health status of the system, there are always two major noise sources. The first one is randomly generated current denoted as I_{Noise} which is directly applied to the neuronal network. The second one is a distortion noise which impacts the I_{app} matrix. Noise and distortion levels were kept the same in all experiments.

Synaptic current is calculated based on the number of activated synaptic connections with the following equation[89,90]:

$$I_{Syn}^{(i,j)} = \sum_{k=1}^{N_{in}^{(i,j)}} \frac{g_{Syn}^{(k)\,(i,j)} \left(E_{Syn}^{(k)} - V_{Post}^{(i,j)} \right)}{1+\exp\left(\frac{V_{Pre}^{(k)}}{S_{Syn}} \right)} \quad \text{(Equation 3)}$$

Every synaptic connection is identified with a superscript (k). The presynaptic voltage of any connection $V_{Pre}^{(k)}$ acts as an activation function with the slope of S_{Syn}. The synaptic reversal potential $E_{Syn}^{(k)}$ determines whether the synapse is excitatory ($E_{Syn} = 0$) or inhibitory ($E_{Syn} = -90$). In this model, all synaptic connections are excitatory. The g_{Syn} determines the strength of the connection between PrSN and PoSN, and defined as:

$$g_{Syn}^{(k)\,(i,j)} = ST1_{Syn}^{(k)\,(i,j)} \left(\eta_{Syn} + g_{WM}^{(m,n)} + g_{SR}^{(i,j)} \right) \quad \text{(Equation 4)}$$

where the default synaptic weight is determined by η_{Syn}, WM activities is included by $g_{WM}^{(m,n)}$ and local SR activities is included by $g_{SR}^{(i,j)}$. The value of g_{WM} is determined by the whole-cell astrocytic activity meaning that when an astrocyte initiates its global activity, it is modulating all the neighboring synaptic connections. The g_{SR} value is limited to the local activity of astrocytes, meaning that whenever it gets activated, all the synaptic connections of the targeted neurons receive this signal, however, its intensity changes based on the synaptic activity. Variable $ST1$ models damage to synapses. In all damage modes, $ST1$ always changes first and then $ST2$ is calculated by averaging $ST1$ values. It should be noted that, in random damage mode, a random value between zero and one is selected for the $ST1$ of the individual connections (k) while in pattern-specific damage mode, the value of $ST1$ is selected for all the connections of a neuron (i, j) based on the position and intensity of the damaging pattern.

The number of output synapses $N_{out}^{(i,j)}$ can be adjusted but, the number of input synapses for each neuron is generated randomly based on the predefined number of output synapses, the radius of connections (r), and the probability of connection (λ). The exponential distribution rate $f_R(r)$ depends on the coordinates of connections which are evaluated by calculating the sine and cosine of an angle (φ) which is uniformly distributed in the range of $[0, 2\pi]$[15]:

$$f_R(r) = \begin{cases} 1/\lambda \exp(-(1/\lambda)r) & r > 0 \\ 0 & r < 0 \end{cases} \quad \text{(Equation 5)}$$

and, the coordinates of PoSNs are determined by[15]:

$$x_{Post} = \lceil x_{Pre} + r\cos(\varphi) \rceil, y_{Post} = \lceil y_{Pre} + r\sin(\varphi) \rceil \quad \text{(Equation 6)}$$

where x_{Pre} and y_{Pre} indicate the coordinates of PrSNs, while x_{Post} and y_{Post} denote the coordinates of PoSNs. Since each neuron can only have one connection to other neurons, the network generation phase constantly check these values to avoid duplicate connections. The final result of Equations 5 and 6 are two matrices called "pre" and "post", indicating the coordinates of PrSNs and PoSNs, respectively. The number of presynaptic connections (N_{in}) can be found in the post matrix. By evaluating the number of activated input synapses with respect to the total number of connections, a concept called Strength of Input (SoI_{Syn}) can be calculated as follows:

$$SoI_{Syn}^{(i,j)} = \frac{\text{Number of } N_{in(Activated)}^{(i,j)}}{\text{Number of } N_{in}^{(i,j)}} \quad \text{(Equation 7)}$$

The condition for considering an input synaptic connection to be activated is to have a synaptic current of higher than 0.001 μA. The number of activated input synapses does not have a linear relation with the firing event. Therefore, fine-tuning this condition is necessary for a given model to ensure accurate results.

$$SoI_{Syn(N)}^{(i,j)} = CA \times \left(SoI_{Syn}^{(i,j)} \right)^{CR} \quad \text{(Equation 8)}$$

where $SoI_{Syn(N)}^{(i,j)}$ is the non-linear value of SoI, $CR = 0.1$ is the compression rate and $CA = 0.8$ is the compression amplitude, which are just two parameters to control the nonlinearity of the SoI signal. This non-linear interaction is also experimentally observed.[68]

In the event of postsynaptic firing, 2AG is released from PoSN impacting all of its presynaptic axonal terminals and nearby astrocytes, and is defined as follows:

$$\frac{d\left(AG^{(i,j)}\right)}{dt} = -\frac{AG^{(i,j)}}{\tau_{AG}} + r_{AG}\delta\left(V_{Post}^{(i,j)} - 30mV\right) \quad \text{(Equation 9)}$$

where $AG^{(i,j)}$ is the amount of 2AG released from the dendritic terminals targeting presynaptic and astrocytic CB1 receptors. r_{AG} is the release rate of 2AG signal and τ_{AG} is the decay rate of 2AG signal. The event of firing is defined by the delta function which indicates the event of a postsynaptic firing.

To model glutamate release, it is typical to select an equation like (Equation 9) with the activation function based on the spiking event of V_{Pre} or V_{Post}. However, considering only firing events as the primary mechanism for releasing glutamate from synapses can lead to two major problems. First, this type of modeling does not account for inadequately released glutamate (inadequate synaptic current) from PrSNs that failed to generate a postsynaptic action potential. Second, any impairment in the synapses would not affect the released glutamate. To address these issues, a new glutamate release equation is proposed, which operates based on the number of activated synapses. The *SoI* signal is a suitable candidate for this purpose, as it encodes the number of activated synapses for each PoSN while still adhering to the quantized principle of neurotransmitter release.[91] This signal is defined as follows:

$$\frac{d\left(Glu^{(i,j)}\right)}{dt} = -\frac{Glu^{(i,j)}}{\tau_{Glu}} + r_{Glu} \times SoI_{Syn}^{(i,j)} \times ST2^{(i,j)} \quad \text{(Equation 10)}$$

where *Glu* indicates the amount of released glutamate from the presynaptic axonal terminal in a synaptic cleft targeting mGluRs on astrocytes and postsynaptic dendritic terminals. The release rate is defined by r_{Glu} and the decay rate is denoted by τ_{Glu}. Variable *ST2* modulates the efficacy of the released glutamate.

Neuron-astrocyte interaction

Interaction of neurons with astrocytes is in the form of released glutamate and 2AG from PrSNs and PoSNs, respectively. To distinguish the efficacy of these neurotransmitters targeting astrocytic receptors, two coefficients are considered. In this way, the total neurotransmitters bind with astrocytes (Ω_{Astro}) can be defined as:

$$Glu \times \gamma_{Glu} + AG \times \gamma_{AG} = \Omega_{Astro} \quad \text{(Equation 11)}$$

The efficacy factors of glutamate (γ_{Glu}) and 2AG (γ_{AG}) in the synaptic clefts play a crucial role in astrocytes' functionality. These factors can depend on various aspects, including the ratio of glutamate and 2AG receptors on astrocytes, the clearance rates, the activation/inactivation characteristics of receptors, and the production rate of IP_3 inside astrocytes. In this model, these factors are finely tuned to enable astrocytes to detect intense neuronal activities through the sufficient release of both neurotransmitters. For example, if one of the released neurotransmitters is significantly lower than the other, astrocytes will not be able to detect intense neuronal activity effectively. Intense neuronal activity is defined by two specific conditions. Once these conditions are met, a fixed value of A_Ω is considered as an input to the astrocyte. The mathematical equation for $A_\Omega(t)$ is as follows[15]:

$$A_\Omega(t) = \begin{cases} A_\Omega & if \left(\sum_{(i,j)\in N_a} \Theta\left(\Omega_{Astro}^{(i,j)} - \Omega_{Thr(global)}\right)\right) \geq F_{Memorize} \times N_a \\ 0 & otherwise \end{cases} \quad \text{(Equation 12)}$$

where Θ is the Heaviside step function and $N_a = 16$ is the number of neurons connected to an astrocyte. Among these neurons, if a fraction $F_{Memorize} = 0.5$ of them (8 out of 16 neurons), have the total bound neurotransmitter (Ω_{Astro}) greater than $\Omega_{Thr(global)} = 0.7\ \mu M$; a fixed value of A_Ω is considered as an input signal for the production of IP_3. This input is retained as long as these conditions are satisfied but limited to t_Ω duration. In this way, noise can contribute to these conditions but, it cannot fulfill it alone. In other words, $F_{Memorize}$ evaluates the synchronicity of the event and $\Omega_{Thr(global)}$ assesses the intensity of that event. These two conditions can be referred to as the "memorize condition" or the "strong synchronous activity of neurons condition". This signal can be summarized into:

$$(J_{Glu} + J_{AG}) = J_\Omega = \begin{cases} A_\Omega(t) & t_0 < t < t_0 + t_\Omega \\ 0 & \text{Otherwise} \end{cases} \quad \text{(Equation 13)}$$

where J_Ω is the input applied to an astrocyte for its IP_3 production with the fixed amplitude of A_Ω in the interval of t_Ω. As it was mentioned before, one of the factors in the delay of the DMS WM model is in satisfying this condition which is the amount of time that it takes to reach the 0.7 μM neurotransmitter bound with an astrocyte by at least half of the neurons near to this cell.

Astrocyte model

All equations in the astrocyte model are solved with the fourth-order Runge-Kutta method using a fixed time step of 0.1 ms. Released neurotransmitters in the tripartite synapses bind with the astrocytic membrane receptors located close to the synapses. This triggers the production of IP_3 in the astrocytes. Ullah model was utilized to calculate this dynamic[92,93]:

$$\frac{d\left(IP_3^{(m,n)}\right)}{dt} = \frac{IP_3^* - IP_3^{(m,n)}}{\tau_{IP_3}} + J_{PLC\delta}^{(m,n)} + J_{\Omega}^{(m,n)} + dif_{IP_3}^{(m,n)}$$

$$J_{PLC\delta} = \frac{v_4([Ca^{2+}]+(1-\alpha)k_4)}{[Ca^{2+}]+k_4} \quad \text{(Equation 14)}$$

where $m, n \in \{1, \ldots, 26\}$ are the astrocyte indices. Parameter IP_3^* indicates the steady-state concentration of the IP_3 and $J_{PLC\delta}$ denotes the IP_3 production by phospholipase Cδ (PLCδ).[75] The input due to the total bound neurotransmitter is defined by J_Ω. An increase in IP_3 concentration in the astrocytes causes the release of Ca^{2+} from internal stores, mostly from the endoplasmic reticulum (ER), to cytosol. The Ullah model[93] was utilized to track changes in the intracellular Ca^{2+} concentration with the difference of adding two variables for Ca^{2+} depletion due to whole-cell and local activities:

$$\frac{d[Ca^{2+}]^{(m,n)}}{dt} = J_{ER}^{(m,n)} + J_{Leak}^{(m,n)} - J_{Pump}^{(m,n)} + J_{in}^{(m,n)} - J_{out}^{(m,n)} + dif_{Ca}^{(m,n)} - \zeta_{Global} W_{Global}^{(m,n)} - \zeta_{Local} W_{Local}^{(m,n)}$$

$$\frac{dh^{(m,n)}}{dt} = a_2\left(d_2\frac{IP_3^{(m,n)}+d_1}{IP_3^{(m,n)}+d_3}\left(1-h^{(m,n)}\right) - [Ca^{2+}]^{(m,n)}h^{(m,n)}\right) \quad \text{(Equation 15)}$$

where W_{Local} and W_{Global} denote the window of local and whole-cell activities, defined in Equations 20 and 25, respectively. ζ_{Global} and ζ_{Local} are efficacy factors for the depletion of Ca^{2+} for whole-cell and local activities, respectively. h is the portion of the activated IP_3 receptors (IP3Rs) on the ER surface. J_{ER} flux is Ca^{2+} flow from the ER to the cytosol by IP3Rs, J_{Pump} is the Ca^{2+} flux pumped back into the ER via the sarco/ER Ca^{2+}-ATPase (SERCA), and J_{Leak} is the leakage current from the ER to the cytosol. J_{in} and J_{out} specify the calcium exchange with extracellular space. These fluxes are expressed as:

$$J_{ER} = c_1 v_1 [Ca^{2+}]^3 h^3 IP_3^3 \frac{\left(\frac{c_0}{c_1} - \left(1+\frac{1}{c_1}\right)[Ca^{2+}]\right)}{((IP_3+d_1)([Ca^{2+}]+d_5))^3}$$

$$J_{Leak} = c_1 v_2\left(\frac{c_0}{c_1} - \left(1+\frac{1}{c_1}\right)[Ca^{2+}]\right)$$

$$J_{Pump} = \frac{v_3[Ca^{2+}]^2}{k_3^2+[Ca^{2+}]^2}$$

$$J_{in} = \frac{v_6 IP_3^2}{k_2^2+IP_3^2}$$

$$J_{out} = k_1[Ca^{2+}] \quad \text{(Equation 16)}$$

The biophysical meaning of all parameters in Equations 14, 15, and 16 are provided in ref.[93,94] Since cortical astrocytes are coupled by Cx43 gap junctions,[95] the diffusion of calcium ions and IP_3 molecules via gap junctions between neighboring astrocytes is modeled with dif_{Ca} and dif_{IP_3} which are expressed as:

$$dif_{Ca}^{(m,n)} = d_{Ca}\left(\Delta[Ca^{2+}]\right)^{(m,n)}$$

$$dif_{IP_3}^{(m,n)} = d_{IP_3}(\Delta IP_3)^{(m,n)} \quad \text{(Equation 17)}$$

where d_{Ca} and d_{IP_3} represent the Ca^{2+} and IP_3 diffusion rates, respectively. Each astrocyte is diffusively coupled with a maximum of four nearest neighbors. $(\Delta[Ca^{2+}]^{(m,n)})$ and $(\Delta IP_3{}^{(m,n)})$ are the discrete Laplace operators that can be expressed in the following equation by replacing the $\mathcal{X}$ variable:

$$(\Delta[\mathcal{X}])^{(m,n)} = \left([\mathcal{X}]^{(m+1,n)} - [\mathcal{X}]^{(m,n)}\right) + \left([\mathcal{X}]^{(m-1,n)} - [\mathcal{X}]^{(m,n)}\right) + \left([\mathcal{X}]^{(m,n+1)} - [\mathcal{X}]^{(m,n)}\right) + \left([\mathcal{X}]^{(m,n-1)} - [\mathcal{X}]^{(m,n)}\right) \quad \text{(Equation 18)}$$

Astrocyte-neuron interaction

The interaction of astrocytes with neurons can be categorized into several types. Astrocytic glutamate-induced potentiation of the excitatory synapse consists of NMDAR-dependent postsynaptic slow inward currents (SICs) generation[66,96] and mGluR-dependent heterosynaptic facilitation of presynaptic glutamate release.[26,28,46] Here only its impact on PrSNs is considered. This effect is divided into two types, local and whole-cell activities for SR and WM mechanisms, respectively.

Self-repairing mechanism (local interaction of astrocytes)

The released 2AG from the PoSN can directly impact the presynaptic axonal terminals. This inhibitory signal is defined as follows:

$$DSE^{(i,j)} = k_{DSE} \times AG^{(i,j)} \quad \text{(Equation 19)}$$

where k_{DSE} is a constant factor to shift the acquired 2AG signal to the desired negative range. On the other hand, the released 2AG and glutamate in tripartite synapses can cause an increase in the calcium concentration of astrocytes. As the intracellular Ca^{2+} of astrocytes reaches a certain level, they can release gliotransmitters targeting mGluRs on presynaptic axonal terminals. This signal is defined as:

$$\frac{d\left(Gli^{(i,j)}_{Local}\right)}{dt} = -\frac{Gli^{(i,j)}_{Local}}{\tau_{Gli}} + r_{Gli} W^{(i,j)}_{Local}$$

$$W^{(i,j)}_{Local} = \Theta\left(\left[Ca^{2+}\right]^{(m,n)} - \left[Ca^{2+}\right]_{Thr(SR)}\right)\left(Sol^{(i,j)}_{Syn(N)}\right)\Theta\left(\Omega^{(i,j)}_{Astro} - \Omega_{Thr(local)}\right) \quad \text{(Equation 20)}$$

where $Gli^{(i,j)}_{Local}$ is the locally-released gliotransmitter from astrocytes, r_{Gli} is the release rate of the gliotransmitter and τ_{Gli} is the clearance time constant. The required calcium threshold for this activity is considered $[Ca^{2+}]_{Thr(SR)} = 0.1\ \mu M$ and modeled by a Heaviside step function Θ. The variable $Sol_{Syn(N)}$ dynamically changes based on the synaptic activities. In accordance with experimental data, this interaction is nonlinear, so the nonlinear form of synaptic activity is employed. The local activity of astrocytes is regulated based on the region that input is stimulating, the potency of the local event ($\Omega^{(i,j)}_{Astro}$), and a nonlinear form of synaptic activity ($Sol^{(i,j)}_{Syn(N)}$). The $\Omega_{Thr(local)} = 0.2\ \mu M$ is the required concentration threshold of neurotransmitters bind with an astrocyte for initiation of local activity of astrocytes.

The fault tolerance of the SR mechanism is integrated into released Gli_{Local} since its calcium condition can be satisfied by the incoming glutamate, 2AG, Ca^{2+}, and IP_3 from the neighboring neurons and astrocytes. The *eSP* signal is the result of released Gli_{Local} and defined as:

$$\frac{d\left(eSP^{(i,j)}\right)}{dt} = -\frac{eSP^{(i,j)}}{\tau_{eSP}} + k_{eSP}\left(Gli^{(i,j)}_{Local}\right) \quad \text{(Equation 21)}$$

where $eSP^{(i,j)}$ indicates the value of eSP for each neuron, k_{eSP} is a constant factor to shift the maximum value of Gli_{Local} to a desired positive range and τ_{eSP} is the decay rate of the eSP signal. Modeling the eSP signal in this way enables the algorithm to distinguish the "off" connections from the "damaged" ones since the deactivation of any synaptic connection leads to a decrease in *Sol*, ensuring the retention of the balance between *DSE* and *eSP* signals in healthy conditions. Therefore, the BoF can be defined as follows:

$$BoF^{(i,j)} = \left(DSE^{(i,j)} + eSP^{(i,j)}\right) + Bias \quad \text{(Equation 22)}$$

Variable $Bias = 1$ is just a bias term to adjust the BoF to the desired range. The *BoF* acts as a control unit where the provided eSP is compared with the *DSE* signal. After acquiring the *BoF* signal, a threshold as a noise margin is defined where if the *BoF* passes the designated limit, a fixed g_{SR} get applied to the neurons. This process is defined as follows:

$$W^{(i,j)}_{SR} = \begin{cases} 1 & BoF^{(i,j)} \geq BoF_{th} \\ 0 & \text{Otherwise} \end{cases}$$

$$g^{(i,j)}_{SR} = \eta_{SR} \times W^{(i,j)}_{SR} \quad \text{(Equation 23)}$$

where $BoF_{th} = Bias + 0.01$ is a noise margin for *BoF*. W_{SR} is a time window that indicates when the SR activities are happening. g_{SR} is the amount of SR activities due to the eSP values overcoming the DSE values. $\eta_{SR} = 0.4$ is a fixed coupling factor, scaling the strength of SR activities. A noise margin is defined in a way to get the minimum SR activities in healthy status. In the BoF-based SR algorithm, excitation happens by receiving the g_{SR} and inhibition happens by not receiving the g_{SR} signal.

Working memory mechanism (whole-cell interaction of astrocytes)

Synchronous WM activity is considered a glutamate-induced potentiation of synaptic facilitation of all synapses belonging to the morphological territory of an astrocyte.[15] It is implemented when the following two conditions are satisfied:

$$W_{WM}\ \text{Conditions}: \begin{cases} \left[Ca^{2+}\right]^{(m,n)} \geq \left[Ca^{2+}\right]_{Thr(WM)} \\ F_{Spike} \geq F_{Recall} \times N_a \end{cases} \quad \text{(Equation 24)}$$

where the fraction of synchronously spiking neurons F_{Spike} encompassed by an astrocyte should be greater than $F_{Recall} = 0.375$ which is 6 out of 16 neurons in this model. Given that the calcium concentration of the nearby astrocyte $[Ca^{2+}]^{(m,n)}$ is greater than the required calcium concentration for a synchronous WM event $[Ca^{2+}]_{Thr(WM)} = 0.15\ \mu M$, a window with constant duration for the WM event ($W_{WM}^{(m,n)}$) will be considered. These concepts can be summarized as:

$$W_{WM}^{(m,n)} = \begin{cases} 1 & t_0 < t \leq t_0 + t_{WM} \\ 0 & \text{Otherwise} \end{cases}$$

$$\frac{d\left(Gli_{Global}^{(m,n)}\right)}{dt} = -\frac{Gli_{Global}^{(m,n)}}{\tau_{Gli}} + r_{Gli} \times W_{Global}^{(m,n)}$$

$$W_{Global}^{(m,n)} = \Theta\left(\left[Ca^{2+}\right]^{(m,n)} - \left[Ca^{2+}\right]_{Thr(WM)}\right) \times W_{WM}^{(m,n)}$$

$$g_{WM}^{(m,n)} = \eta_{WM} \times Gli_{Global}^{(m,n)} \quad \text{(Equation 25)}$$

Where $Gli_{Global}^{(m,n)}$ is the whole-cell glutamate release of astrocytes. g_{WM} is the astrocytes whole-cell activity for WM mechanism which affects all synaptic connections of neighboring neurons. The strength of this modulation is defined by the coupling factor $\eta_{WM} = 0.4$. This modulation happens within the time window of W_{WM} where the t_0 is the exact moment of detecting a synchronous activity with $F_{Spike} > 6$ given that the nearby astrocyte has $[Ca^{2+}] \geq 0.15\ \mu M$. The working memory window W_{WM} lasts for the duration of the applied input sample (0.15 s) plus the desired extra time without input (0.1 s) which results in $t_{WM} = 250\ ms$.

Correlation

Correlation is computed using the following equations taken from[15]:

$$t_{train}^{i} = i \cdot \tau_{11} + (i-1)\tau_{12},$$

$$t_{test}^{j,i} = t_{train}^{i} + \tau_{shift} + j \cdot \tau_{21} + (j-1)\tau_{22}$$

$$C = \frac{1}{K!}\sum_{p}\sum_{1}^{K}\left[t_{test}^{p_i,i} - t_{train}^{i} < \tau_{Ca}\right] =$$

$$\frac{1}{K!}\sum_{1}^{K}\sum_{p}\left[t_{test}^{p_i,i} - t_{train}^{i} < \tau_{Ca}\right] =$$

$$\frac{(K-1)!}{K!}\sum_{1}^{K}\sum_{j=1}^{K}\left[t_{test}^{j,i} - t_{train}^{i} < \tau_{Ca}\right] \quad \text{(Equation 26)}$$

where τ_{11} is the duration of samples in the training phase, τ_{12} is the duration of sample interval in the training phase, τ_{21} is the duration of samples in the testing phase, τ_{22} is the duration of samples interval in the testing phase, τ_{shift} is the delay between train and test phase, τ_{ca} is the duration of whole-cell astrocytic activity, t_{train}^{i} is the finish time of i-th sample in training, and $t_{test}^{j,i}$ is the finish time of WM interval of i-th sample in testing.[15] In summary, this formula compares the neuronal activity with respect to the shape of a sample in the training and testing phases.